

Neighborhood-Level Nitrogen Dioxide Inequalities Contribute to Surface Ozone Variability in Houston, Texas

Isabella M. Dressel, Sixuan Zhang, Mary Angelique G. Demetillo, Shan Yu, Kimberly Fields, Laura M. Judd, Caroline R. Nowlan, Kang Sun, Alexander Kotsakis, Alexander J. Turner, and Sally E. Pusede*



Cite This: <https://doi.org/10.1021/acsestair.4c00009>



Read Online

ACCESS |



Metrics & More



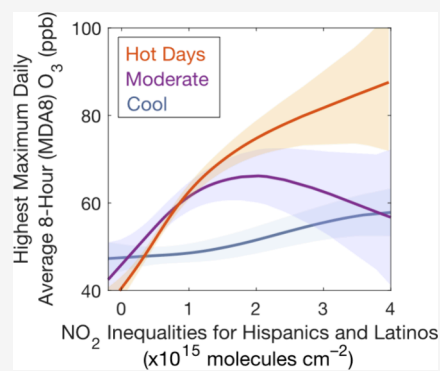
Article Recommendations



Supporting Information

ABSTRACT: In Houston, Texas, nitrogen dioxide (NO_2) air pollution disproportionately affects Black, Latinx, and Asian communities, and high ozone (O_3) days are frequent. There is limited knowledge of how NO_2 inequalities vary in urban air quality contexts, in part from the lack of time-varying neighborhood-level NO_2 measurements. First, we demonstrate that daily Tropospheric Monitoring Instrument (TROPOMI) NO_2 tropospheric vertical column densities (TVCDs) resolve a major portion of census tract-scale NO_2 inequalities in Houston, comparing NO_2 inequalities based on TROPOMI TVCDs and spatiotemporally coincident airborne remote sensing (250 m \times 560 m) from the NASA TRacking Aerosol Convection Experiment–Air Quality (TRACER-AQ). We further evaluate the application of daily TROPOMI TVCDs to census tract-scale NO_2 inequalities (May 2018–November 2022). This includes explaining differences between mean daily NO_2 inequalities and those based on TVCDs oversampled to $0.01^\circ \times 0.01^\circ$ and showing daily NO_2 column–surface relationships weaken as a function of observation separation distance. Second, census tract-scale NO_2 inequalities, city-wide high O_3 , and mesoscale airflows are found to covary using principal component and cluster analysis. A generalized additive model of O_3 mixing ratios versus NO_2 inequalities reproduces established nonlinear relationships between O_3 production and NO_2 concentrations, providing observational evidence that neighborhood-level NO_2 inequalities and O_3 are coupled. Consequently, emissions controls specifically in Black, Latinx, and Asian communities will have co-benefits, reducing both NO_2 disparities and high O_3 days city wide.

KEYWORDS: Nitrogen dioxide, ozone, TROPOMI, urban air pollution, environmental racism



INTRODUCTION

Houston, Texas is a large U.S. city and center for petrochemical refining that faces multiple air quality challenges. Historical and contemporary policies and practices continue to disproportionately offload the environmental costs of industry and transportation on Black, Latinx, and Asian communities,^{1,2} causing measurable inequalities in the distribution of nitrogen dioxide (NO_2) and other primary pollutants.^{3–9} Houston is also currently ranked among the top ten most ozone (O_3) polluted cities in the U.S., with residents experiencing frequent exceedances of health-based O_3 standards city wide.¹⁰ Recent analytical advances have produced more spatially detailed descriptions of neighborhood-level urban air pollution inequalities,^{11–15} including for NO_2 .^{16–18} However, enhanced spatial information has generally relied on time-averaged and/or short-duration observations, representing conditions that potentially infrequently occur and limiting our understanding of relationships between NO_2 inequalities and broader urban air quality issues such as O_3 . This has policy relevance as states have regulatory authority around O_3 compliance that they often lack or decline to use regarding air pollution environmental injustice.

NO_2 is a criteria pollutant regulated by the U.S. Environmental Protection Agency (EPA). NO_2 is a primary pollutant (or pseudo-primary pollutant) with a summertime atmospheric lifetime as short as a few hours. Primary pollutants are highly spatiotemporally variable, exhibiting atmospheric dispersion gradients of hundreds of meters to 1–2 km.^{11,19,20} NO_2 is emitted as NO_x ($\equiv \text{NO} + \text{NO}_2$), with vehicles and electricity generation being major NO_x sources in U.S. cities.^{21–23} Houston is also a global hub for petrochemical manufacturing, where refineries and industrial activities contribute a large portion of NO_x emissions,^{24–26} especially in the Houston Ship Channel,^{24–26} a residential and industrial area along the Buffalo Bayou River, connecting downtown to Galveston Bay and the Gulf of Mexico (Figure 1). Associated with numerous

Received: January 20, 2024

Revised: July 19, 2024

Accepted: July 19, 2024

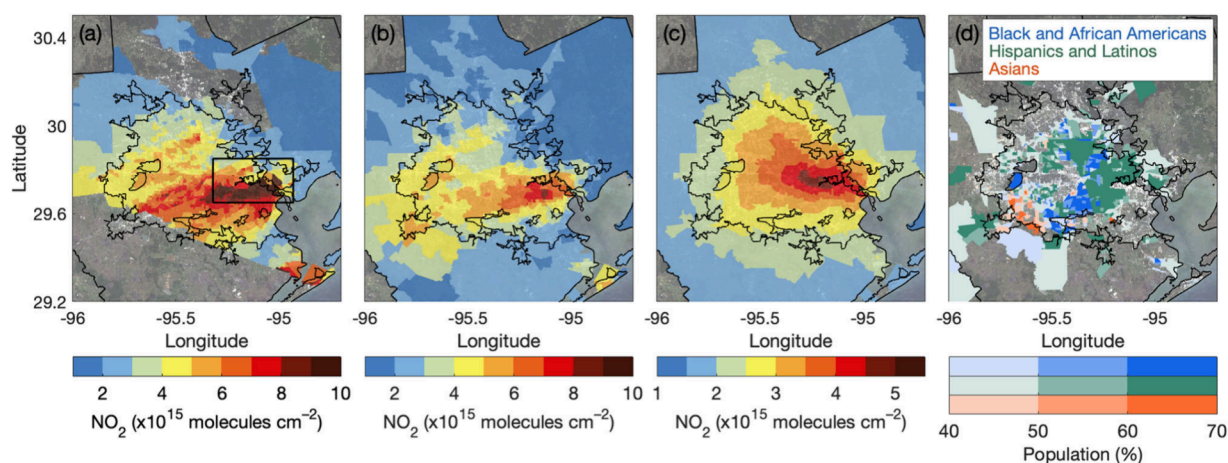


Figure 1. Example of census tract-scale GCAS NO_2 columns (molecules cm^{-2}) collected on 25 September 2021 at 2–5 pm (a), TROPOMI TVCDs on the same day, with a mean pixel size of $21 \pm 0.6 \text{ km}^2$ (b), and oversampled TROPOMI TVCDs ($0.01^\circ \times 0.01^\circ$) over May 2018–November 2022 (c). Also shown, the percent population for the largest race-ethnicity group in each census tract for Black and African Americans (blue), Hispanics and Latinos (green), and Asians (orange) (d). The inner and outer black lines are the Urbanized Area (UA) and Metropolitan Statistical Area (MSA) boundaries, respectively. The thick black box is the Houston Ship Channel (a). Background map data: Landsat 8 composite (January 2017–June 2018). Corresponding wind conditions are presented in Figure S1.

adverse^{27–31} and unequal health impacts,²⁸ NO_2 is a common proxy for toxic combustion and traffic air pollution mixtures in health studies.³² High-volume roadways and heavy-duty diesel truck traffic overburden communities of color,^{33,34} and living near roadways is linked to asthma-related urgent medical visits, pediatric asthma, preeclampsia and preterm birth, and cardiac and pulmonary mortality.^{35–40}

Neighborhood-level NO_2 inequalities with race and ethnicity can be observed from space using the TROPOspheric Monitoring Instrument (TROPOMI).^{3,16,41–45} This was first demonstrated by Demetillo et al.,³ who showed relative census tract-scale NO_2 inequalities based on TROPOMI tropospheric vertical column densities (TVCDs) oversampled to $0.01^\circ \times 0.01^\circ$ agreed with results from fine-scale ($250 \text{ m} \times 500 \text{ m}$) airborne remote sensing during the NASA Deriving Information on Surface Conditions from Column and VERTically Resolved Observations Relevant to Air Quality (DISCOVER-AQ) in Houston. In addition, spatial patterns in oversampled TROPOMI TVCDs reflected NO_2 distributions at the surface, a conclusion based on comparisons with in-situ aircraft NO_2 vertical profiles from DISCOVER-AQ and surface measurements.³ In a subsequent analysis of 52 U.S. cities, Demetillo et al.¹⁶ reported oversampled TROPOMI NO_2 inequalities were invariant with urban racial segregation structure,³⁴ meaning that TROPOMI resolves inter-tract NO_2 differences even when segregated tracts do not spatially aggregate into larger regions. Dressel et al.⁴¹ found mean daily TROPOMI observations ($3.5 \text{ km} \times 5.5 \text{ km}$ at nadir) without oversampling also captured a majority of tract-scale NO_2 inequalities compared to fine-scale ($250 \text{ m} \times 250 \text{ m}$) airborne remote sensing and agreed with relative NO_2 inequalities based on TVCDs oversampled to $0.01^\circ \times 0.01^\circ$ to within associated uncertainties, at least in New York City, New York and Newark, New Jersey. Daily NO_2 inequalities, when uncertainties are well-characterized, can be analyzed statistically and situated within our broader understanding of urban air quality.⁴¹

NO_2 is an O_3 precursor and temporary O_3 reservoir ($\text{O}_x \equiv \text{NO}_2 + \text{O}_3$), with O_3 production chemistry varying nonlinearly with NO_2 and the reactivity of volatile organic compounds

(VOCs) with hydroxyl radical (OH). O_3 pollution in Houston is attributed in large part to the combination of high NO_x and reactive VOC emissions by industries in the Ship Channel and gulf breeze airflows.^{26,46–51} While O_3 air quality has improved,^{52–54} exceedances of the health-based maximum daily average 8-h (MDA8) O_3 National Ambient Air Quality Standard (NAAQS) of 70 ppb are frequent, with 141 exceedance days in the Houston Metropolitan Statistical Area (MSA) over May 2018–November 2022 (our study period). O_3 is a secondary and intermediately long-lived pollutant. As a result, O_3 exhibits less intraurban heterogeneity than NO_2 and is not generally associated with neighborhood-level disparities.⁵⁵ However, because NO_2 and VOC concentrations are spatiotemporally variable, O_3 production (PO_3) chemistry is as well,^{56–58} with NO_2 inequalities and city-wide O_3 potentially coupled. In Houston, the largest NO_2 inequalities during DISCOVER-AQ corresponded to a severe O_3 event with MDA8 O_3 of 124 ppb (LaPorte Sylvan Beach, 25 September 2013).³ In New York City–Newark, tract-scale NO_2 inequalities were positively associated with summertime MDA8 O_3 (2018–2021), with Spearman correlation coefficients of 0.41–0.55 for different population groups.⁴¹

Here, we describe census tract-scale TROPOMI NO_2 inequalities and investigate relationships with MDA8 O_3 in Houston. As a first step, we evaluate daily TROPOMI NO_2 inequalities with race-ethnicity, advancing our understanding of the application of mean daily TROPOMI NO_2 TVCDs to NO_2 inequalities developed in New York City–Newark.⁴¹ We compare daily TROPOMI NO_2 inequalities against measurements of spatiotemporally coincident airborne remote sensing ($250 \text{ m} \times 560 \text{ m}$) during the NASA TRacking Aerosol Convection Experiment–Air Quality (TRACER-AQ) in September 2021, discuss differences between relative and absolute mean daily and oversampled TROPOMI NO_2 inequalities, and present column-surface relationships as a function of measurement separation distance and surface wind conditions. Second, we statistically analyze TROPOMI NO_2 inequalities (May 2018–November 2022), interpreting covariations between neighborhood-level NO_2 inequalities,

overall NO₂ pollution, and urban O₃ air quality in ways that have policy implications.

MEASUREMENTS AND METHODS

TROPOMI. TROPOMI is a hyperspectral spectrometer onboard the sun-synchronous European Space Agency Copernicus Sentinel-5 Precursor (S-5P) satellite.^{59,60} NO₂ is retrieved by fitting the 405–465 nm spectral band based on an updated Dutch OMI (Ozone Monitoring Instrument) NO₂ (DOMINO) algorithm and work from the Quality Assurance for Essential Climate Variables project.^{61–65} NO₂ observations are converted to TVCDs via an air mass factor (AMF), which relies on spatially and temporally coarse inputs, e.g., clouds, surface albedo, and NO₂ profile shape, that can bias NO₂ TVCDs low under high NO₂ conditions.⁶⁶ The application of TROPOMI NO₂ TVCDs to census tract-scale NO₂ inequalities has been evaluated through comparison with airborne remote sensing that resolves NO₂ distance decay gradients, both in terms of TVCDs first oversampled to 0.01° × 0.01°⁶³ and daily TVCDs,⁴¹ with TROPOMI capturing similar relative but lower absolute population-weighted census tract-scale NO₂ inequalities. While the sensitivity of TROPOMI is lower near the surface,^{67,68} there are no physical processes in the free troposphere that maintain intraurban gradients corresponding to neighborhood-level race-ethnicity. TROPOMI TVCDs have been shown to reflect intraurban spatiotemporal NO₂ variability at the surface, a critical analytical requirement for informing decision making around environmental racism.^{3,16,41} Based on 144 in-situ NO₂ vertical profiles throughout Houston from DISCOVER-AQ, Demetillo et al.³ reported that the slope of the linear fit between the measured full column (extending up to 3 km) and NO₂ column within the convective boundary layer was 0.98 ± 0.15 (*r* = 0.99), with no significant location-specific differences. Multiple authors have shown TROPOMI and OMI NO₂ TVCDs correlate with surface-level nitrogen dioxide (NO₂^{*}) measurements and, more importantly, that correlation coefficients decrease with increasing spatial separation between columns and monitors on the scales of NO₂ spatial variability.^{3,16,41,69}

From 1 May 2018 to 5 August 2019, the TROPOMI nadir spatial resolution was 3.5 km × 7 km; from 6 August 2019 to present, the nadir spatial resolution improved to 3.5 km × 5.5 km.⁷⁰ The S-5P satellite crosses the equator at ~1:30 pm local time (LT) and overflies Houston at 12–3 pm LT, typically once but occasionally twice daily. When there are two TROPOMI overpasses over Houston on the same day, we use the first overflight only. We use current Level 2 NO₂ TVCDs (version 02.04.00) with quality assurance values >0.75, as recommended,⁷¹ from operationally reprocessed (RPRO, collection identified: '03', 1 May 2018–25 July 2022) and offline (OFFL, 26 July 2022–30 November 2022) products. A key update in version 02.04.00 is the use of a surface albedo climatology derived from TROPOMI observations rather than the coarse spatial resolution OMI surface albedo climatology (0.5° × 0.5°).⁷¹ TROPOMI NO₂ inequalities can be sensitive to product version; for example, Dressel et al.⁴¹ found census tract-scale NO₂ inequalities based on NO₂ TVCDs reprocessed on the S-5P Products Algorithm Laboratory (SSP-PAL) system were 3–6 points (10–20%) higher over the New York City–Newark urbanized area (UA) than those computed using a then current version of operational product (version 01.02.02). We compared NO₂ inequalities using version 02.04.00 (RPRO) and SSP-PAL

reprocessed TVCDs over January–December 2019 but find results were statistically indistinguishable.

GCAS. The Geostationary Coastal and Air Pollution Events (GEO-CAPE) Airborne Simulator (GCAS) makes hyperspectral nadir-looking measurements of backscattered solar radiation in the ultraviolet and visible in two channels at wavelengths 300–490 nm (optimized for air quality) and 480–900 nm (optimized for ocean color).⁷² Each channel uses a two-dimensional (2D) charge-coupled device (CCD) array detector, where one CCD dimension provides spectral coverage and the other the cross-track spatial coverage across a ~45° field of view in the air quality channel. GCAS was developed as a technology-demonstration instrument for the GEOstationary Coastal and Air Pollution Events (GEO-CAPE) decadal survey and functions as a satellite analog in NASA airborne research. GCAS NO₂ column retrievals are validated over urban areas and consist of a two-step approach similar to algorithms used for other major satellite instruments, including TROPOMI.^{73–75} Briefly, NO₂ differential slant columns are retrieved fitting across 425–460 nm using the QDOAS spectral fitting package⁷⁶ and a reference spectrum measured at a nearby location away from NO_x emissions sources. The AMF is largely a function of viewing and solar geometries, surface reflectance, and atmospheric and trace gas vertical profiles.^{73,77} GCAS retrievals for TRACER-AQ use the NASA GEOS-CF model analyses (0.25° × 0.25°).⁷⁸ Other components of the retrieval follow Judd et al.,⁷⁷ where column uncertainties over New York City–Newark were ±25% and unbiased compared to coincident Pandora measurements, ground-based total NO₂ columns with relatively low uncertainties from AMFs that do not vary with NO₂ vertical profile shape or surface albedo.⁷⁹ During TRACER-AQ, GCAS NO₂ columns were averaged to 250 m (cross-track) × 560 m (along track). GCAS flew onboard the NASA Johnson Space Center Gulfstream V (JSC GV) research aircraft on 11 days in September 2021. We use measurements from the 27 cloud-free flights sampling at least 60% of census tracts in the Houston MSA (Table S1). GCAS flew a repeated flight pattern in the morning (~9–11:30 am LT), midday (~11:30 am–2 pm LT), and afternoon (~2:30–5 pm LT), sampling 83 ± 4% (±1σ) of tracts with similar, but not identical, demographics to the MSA (Tables S2–S3).

Surface NO₂^{*}, O₃, and Meteorological Measurements. NO₂^{*} observations are collected at 23 stations across the MSA (Figure S2a) and provided through the U.S. EPA Air Quality System.⁸⁰ NO₂^{*} is mostly measured by decomposing NO₂ to NO over a heated molybdenum catalyst and detecting NO by chemiluminescence, a technique with a known positive interference from other nitrogen compounds, which also thermally decompose across the catalyst at non-unity efficiency.^{81–83} The term NO₂^{*} acknowledges this interference, which, while affecting accuracy, has a smaller effect on precision.⁸⁴ Two stations in the MSA are near-roadway monitors. We use O₃ mixing ratios measured at 21 stations, many of which also house NO₂^{*} instruments (Figure S2b), converted to MDA8 O₃. We use 1-h measurements of wind speed (resultant), wind direction, and air temperature and daily maximum temperatures collected at 23 stations (Figure S2c) with observations on at least 50% of days during O₃ season, defined in Houston as March–November,⁸⁵ when MDA8 O₃ NAAQS exceedances are most likely to occur.

Census Tract-Scale Inequalities. We calculate area-weighted mean NO₂ TVCDs within 2020 census tract

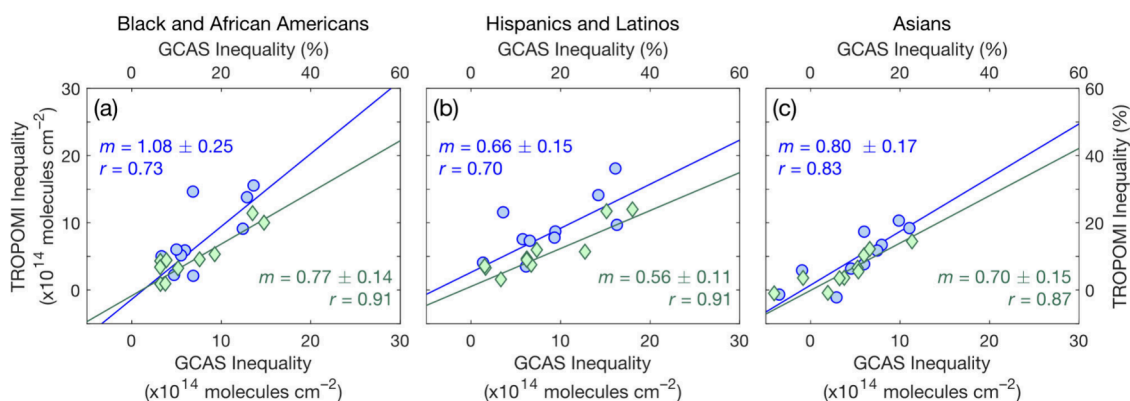


Figure 2. Spatiotemporally coincident (± 30 min) relative (%) (blue circles) and absolute (molecules cm^{-2}) (green diamonds) GCAS and TROPOMI NO_2 inequalities during TRACER-AQ for Black and African Americans (a), Hispanics and Latinos (b), and Asians (c) in comparison to non-Hispanic/Latino whites with slopes (m), based on an unweighted bivariate linear regression, and Pearson correlation coefficients (r) of relative (blue) and absolute (green) inequalities.

polygons across the Houston UA and MSA and population weight tract-average TVCDs using race and ethnicity data from the U.S. Census 5-year 2020 American Community Survey (ACS). The ACS subsamples census unit populations and applies a complex weighting process to account for variability in tract-level sampling rates and differential group response rates. The weighting process prioritizes accuracy over precision, which we manage using population-weighting and aggregation across the UA and MSA.^{86,87} Tract-scale NO_2 inequalities with race-ethnicity are reported as relative (%) and absolute (molecules cm^{-2}) differences between population-weighted NO_2 TVCDs (eq S1^{3,18,88}) for non-Hispanic/Latino Black and African Americans, Hispanics and Latinos of all races, and non-Hispanic/Latino Asians compared to non-Hispanic/Latino whites in tracts with populations equal to or greater than the mean across tracts with observations. NO_2 differences with race and ethnicity are treated as a proxy for racism.

RESULTS AND DISCUSSION

Evaluating Daily TROPOMI NO_2 Inequalities in Houston, Texas. We first compare spatially and temporally coincident daily census tract-scale TROPOMI NO_2 inequalities against those computed using GCAS NO_2 columns, which have sufficient spatial resolution to observe NO_2 dispersion gradients. Correspondence between daily TROPOMI and GCAS inequalities is described using Pearson correlation coefficients and slopes derived from an unweighted bivariate linear regression of simultaneous observations, defined as occurring within ± 30 min (Figure 2). TROPOMI and GCAS NO_2 inequalities are strongly correlated, with r values of 0.70–0.83 (relative) and 0.87–0.91 (absolute), indicating daily TROPOMI NO_2 TVCDs reflect the variability of spatially detailed GCAS observations day to day. Regression slopes are 0.66 ± 0.15 to 1.08 ± 0.25 for relative and 0.56 ± 0.11 to 0.77 ± 0.14 for absolute inequalities; therefore, daily TROPOMI NO_2 TVCDs capture a major portion of tract-scale inequalities in Houston. Slopes for relative inequalities are larger than for absolute inequalities, with relative differences easier to distinguish using measurements coarser than distance decay gradients. This is consistent with results from daily observations in New York City–Newark⁴¹ and reinforces conclusions based on oversampled TVCDs in Houston by Demetillo et al.,³ where TROPOMI resolved comparable

relative but lower absolute inequalities than GCAS during DISCOVER-AQ.

We test the sensitivity of daily TROPOMI census tract-scale NO_2 inequalities to TROPOMI observation spatial resolution by comparing NO_2 inequalities across the natural variability in daily mean TROPOMI pixel size, ranging 20–89 km^2 with a mean of 39 ± 16 km^2 ($\pm 1\sigma$ standard deviation) UA wide (May 2018–November 2022). Because daily inequalities are sensitive to observation coverage, we first remove days with NO_2 observations in fewer than 20% of tracts in the domain (discussed below). We group observations according to thresholds defined by pixel-size quintiles, comparing mean inequalities for each threshold to those derived from the smallest 20% of pixels using 95% confidence intervals from bootstrapped distributions sampled with replacement 10^4 times (Table S4). We do not observe statistically significant differences in mean daily TROPOMI inequalities outside of the 95% confidence intervals compared to the smallest pixels. The lack of pixel area dependence suggests most city-wide NO_2 inequalities, and those that are observed by TROPOMI, are driven by spatially clustered NO_x sources. TROPOMI pixels are larger than the length scales of individual dispersion gradients; however, when NO_x sources are clustered into source regions, their gradients also spatially aggregate. TROPOMI resolves NO_2 gradients on the scale of these source regions, if not individual sources, with the latter causing the information loss compared to GCAS.

Observed NO_2 inequalities based on TVCDs are sensitive to the number of census tracts with NO_2 measurements across the domain (UA or MSA).⁴¹ When observation coverage is low, inequalities tend to be based on TVCDs in census tracts less representative of city-wide demographics. In this case, census tracts where high numbers of residents are in population groups in the majority with respect to city area (not necessarily population count) are overrepresented in the calculation. The net effect is that population-weighted inequalities are based on census tracts that have higher populations of non-Hispanic whites than in the domain on average. In New York City–Newark, Dressel et al.⁴¹ found low observation coverage biased NO_2 inequalities low by 6–7 percentage points and, as a result, identified minimum coverage threshold requirements for daily mean NO_2 inequalities. We test sensitivity of mean daily TROPOMI NO_2 inequalities in Houston, first applying a minimum coverage

Table 1. Mean Daily TROPOMI NO₂ Inequalities at the MSA and UA Level (May 2018–November 2022) on Days Meeting Observation Coverage Thresholds, Inequalities Based on TROPOMI NO₂ TVCDs Oversampled to 0.01° × 0.01°, 0.02° × 0.02°, 0.04° × 0.04°, and 0.06° × 0.06°, and Average Inequalities of the 15 TROPOMI Orbit Patterns That Cover the Houston UA Separately from Means and Oversampled TVCDs (0.01° × 0.01°)^a

| | Mean Daily TROPOMI | | Oversampled TROPOMI | | | | | Separately by TROPOMI Orbit | |
|-----------------------------|---|-----------|---------------------|---------------|---------------|---------------|---------------|-----------------------------|-----------------------------|
| | MSA | UA | MSA | | UA | | | UA | |
| | | | 0.01° × 0.01° | 0.01° × 0.01° | 0.02° × 0.02° | 0.04° × 0.04° | 0.06° × 0.06° | Mean | Oversampled (0.01° × 0.01°) |
| | Relative Inequalities (%) | | | | | | | | |
| Black and African Americans | 17 ± 1 | 8 ± 1 | 18 ± 1 | 9 ± 1 | 9 ± 1 | 8 ± 1 | 8 ± 1 | 9 ± 1 | 9 ± 1 |
| Hispanics and Latinos | 23 ± 1 | 16 ± 1 | 25 ± 1 | 17 ± 1 | 17 ± 1 | 17 ± 1 | 16 ± 1 | 18 ± 1 | 16 ± 1 |
| Asians | 9 ± 1 | -1 ± 1 | 11 ± 1 | 0 ± 1 | 1 ± 1 | 1 ± 1 | 2 ± 1 | 4 ± 1 | 2 ± 1 |
| | Absolute Inequalities (×10 ¹⁴ molecules cm ⁻²) | | | | | | | | |
| Black and African Americans | 6.4 ± 0.5 | 3.6 ± 0.3 | 5.0 ± 0.3 | 2.7 ± 0.3 | 2.7 ± 0.3 | 2.6 ± 0.3 | 2.6 ± 0.4 | 3.7 ± 0.5 | 2.8 ± 0.4 |
| Hispanics and Latinos | 8.8 ± 0.5 | 6.8 ± 0.4 | 7.2 ± 0.4 | 5.4 ± 0.3 | 5.4 ± 0.3 | 5.3 ± 0.3 | 5.2 ± 0.4 | 7.3 ± 0.5 | 5.3 ± 0.4 |
| Asians | 3.7 ± 0.4 | 0.3 ± 0.4 | 2.9 ± 0.3 | 0.1 ± 0.3 | 0.1 ± 0.3 | 0.4 ± 0.4 | 0.5 ± 0.4 | 0.2 ± 0.5 | 0.4 ± 0.4 |

^aUncertainties are expressed as standard mean errors.

requirement of 20% of census tract with observations, then binning daily TVCDs by >20%, >40%, >60%, and >80% census tracts with observations. When bootstrap 95% confidence intervals (calculated with replacement 10⁴ times) for a lower coverage bin do not overlap with the 95% confidence interval for the >80% coverage bin, we identify a significant difference between inequalities. We select thresholds separately for each metric as the lowest coverage bin without a significant difference. Coverage thresholds range 20–40% for relative and absolute inequalities for each metric (Table S5) and are applied throughout. Mean daily TROPOMI NO₂ inequalities in Houston exhibit less observational coverage sensitivity than in New York City–Newark.⁴¹

We compare mean daily NO₂ inequalities to results based on NO₂ TVCDs on the same subset of days oversampled to 0.01° × 0.01° (~1 km × 1 km) using a physics-based algorithm⁸⁹ prior to census tract averaging (Table 1). Oversampling averages measurements over time with large and overlapping pixels to a finer grid, allowing sub-pixel-scale spatial features to be recovered.⁸⁹ The oversampling approach used here treats pixel-level observations as sensitivity distributions using a generalized two-dimensional super Gaussian spatial response function, appropriate for imaging grating spectrometers like TROPOMI. Relative mean daily and oversampled NO₂ inequalities are equal to within associated uncertainties; however, absolute NO₂ inequalities in mean daily TVCDs, which are already low relative to fine-scale airborne remote sensing (Figure 2), are as much as ~30% higher than oversampled TVCDs. We see multiple possible explanations for this: oversampling is not enhancing spatial gradients relevant to describing census tract-scale NO₂ inequality, which is instead determined by the spatial resolving power set by pixel size; there is limited NO₂ variability on scales of 1–4 km as relevant to NO₂ inequalities; and/or there is compensating information in the daily inequalities lost through time averaging.

First, we compare NO₂ inequalities based on oversampled TVCDs over a range of grid sizes, finding no significant differences in relative or absolute inequalities when we oversample to 0.01° × 0.01°, 0.02° × 0.02°, 0.04° × 0.04°

(the approximate TROPOMI nadir resolution), and 0.06° × 0.06°. In an analysis of 52 major U.S. UAs, Demetillo et al.¹⁶ also reported small differences in relative and absolute census tract-scale NO₂ inequalities using TROPOMI TVCDs oversampled to 0.01° × 0.01° and 0.04° × 0.04°, with the exceptions of the narrow coastal Californian cities of Oakland, San Diego, and San Francisco, where NO₂ inequalities based on TVCDs oversampled to 0.04° × 0.04° were biased low by 8–22% compared to TVCDs oversampled to 0.01° × 0.01°, suggesting oversampling enhances spatial gradients from coarser pixels when that variability exists.¹⁶ Second, we take advantage of the natural variability in TROPOMI pixel orientations, separately comparing NO₂ inequalities based on oversampled TVCDs to mean NO₂ TVCDs collected within individual S-SP orbits, thus eliminating the oversampling pixel overlap requirement. On average, for the 15 S-SP satellite orbits that fully cover the Houston UA, relative NO₂ inequalities from oversampled and mean NO₂ TVCDs are similar; however, absolute NO₂ inequalities of mean TVCDs are ~30% higher than oversampled TVCDs for Black and African Americans and Hispanics and Latinos (Table 1; Table S6), indicating the information loss is not simply because of time averaging, but smoothing during oversampling. In Figure 3, we compare mean and median distributions of tract-scale daily and oversampled (0.01° × 0.01°) TROPOMI TVCDs, fit assuming distributions are lognormal as is characteristic for NO₂. Mean daily measurements span a wider range of NO₂ conditions and retain more observations in the high tail of the distribution than oversampled TVCDs, with high NO₂ values driving inequalities. Sun et al.⁸⁹ report that oversampling, including with the physics-based algorithm used here, is more accurate when the grid is fine relative to a gradient with a smooth spatial response, for example, a city edge, while pixel means are more accurate for coarse grids and sharper spatial responses. Our results suggest absolute census tract-scale NO₂ inequalities are more accurately represented using means, with TROPOMI pixels and typical oversampling grids being large relative to scale of dispersion. Research using oversampled NO₂ TVCDs to identify NO_x point sources and infer NO_x emissions and NO₂ lifetimes have improved absolute estimates by rotating spatially variable NO₂ plumes to a common wind

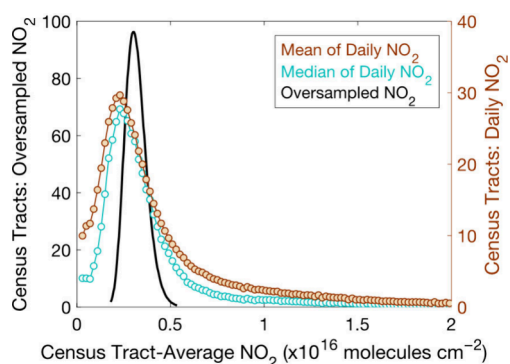


Figure 3. Lognormal distributions of census tract-average TROPOMI NO_2 TVCDs in the Houston UA (May 2018–November 2022). Left axis: TVCDs oversampled to $0.01^\circ \times 0.01^\circ$ (black line). Right axis: mean (brown filled circles) and median (cyan open circles) of distributions of daily observations.

direction,^{90–93} an aspatial solution not applicable to describing census tract-scale NO_2 inequalities, although potentially useful for informing related decision-making.

To describe spatiotemporal variability in column-surface relationships, we compare daily tract-average TROPOMI TVCDs and daytime (12–3 pm LT) NO_2^* surface mixing ratios across the MSA as a function of their separation distance using Pearson correlation coefficients (r) over May 2018–November 2022 (Figure 4).^{3,16,41,69} We require NO_2^* mixing

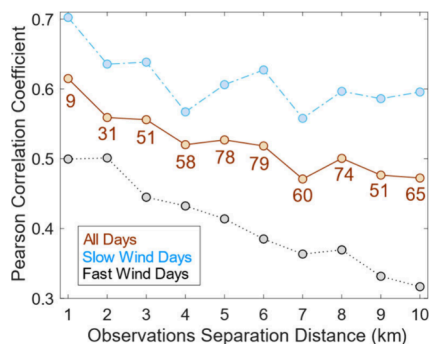


Figure 4. Median daily Pearson correlation coefficients between tract-averaged NO_2 TVCDs and surface NO_2^* mixing ratios as a function of observation separation distance (km) on all days over May 2018–November 2022 (brown solid line) and on days in low (light blue dashed line) and high (black dotted line) quartile winds. We indicate the mean number of census tracts in the daily correlation at that distance each day, with similar statistics on low and high wind days.

ratio data at four or more monitors in each 1-km distance bin per day and exclude near-roadway monitors, which are subject to hyperlocal effects. Surface NO_2^* and directly overhead TVCDs (defined as tract center points within 1 km of an NO_2^* monitor) are strongly correlated, with median r values of 0.62. Correlation coefficients decrease as the distance between observations increases, falling to 0.54 on average when tract-average TVCDs are 2–6 km from the nearest monitor and 0.48 at 7–10 km. This r -distance dependence indicates spatial variability in daily TROPOMI TVCDs follows NO_2^* patterns at the surface, with r decreases at 1–2 km consistent with length scales of NO_2 dispersion gradients. If we consider uncertainties as standard mean errors based on the number of days with observations included in the daily average, uncertainties in r are typically ± 0.01 and mean differences in

r with distance are significant. However, column-surface relationships are variable daily, with standard deviations (1σ) of ~ 0.3 in each distance bin. Daily correlation coefficients are lower than for oversampled TROPOMI TVCDs as reported in Demetillo et al.,³ especially at 1 km, meaning time averaging masks temporal variability in column-surface agreement. We also sort daily observations in the highest ($>3.9 \text{ m s}^{-1}$) and lowest ($<2 \text{ m s}^{-1}$) UA-wide mean daytime (12–3 pm LT) surface wind quartiles as a function of distance, as wind is a physical control over the inter-tract NO_2 distribution. Daily column-surface correlations covary with wind speeds physically realistically, with stronger r values for slower winds and smaller r values with faster winds at all observation separation distances.

Daily NO_2 Inequalities. We calculate daily TROPOMI census tract-average NO_2 inequalities over May 2018–September 2022 across the Houston UA and MSA (Table 1; Figure 5). Mean daily UA-level population-weighted NO_2 TVCDs are $8 \pm 1\%$ and $16 \pm 1\%$ higher for Black and African Americans and Hispanics and Latinos compared to non-Hispanic/Latino whites, respectively. Neighborhoods near the Houston Ship Channel (Figure 1) with large populations of Black and African Americans and Hispanics and Latinos, e.g., Pasadena, Fifth Ward, Harrisburg/Manchester, and Galena Park, often have the highest NO_2 concentrations. Mean population-weighted NO_2 TVCDs for each group including non-Hispanic/Latino whites are shown in Table S7. Inequalities for Black and African Americans and Hispanics and Latinos increase to $17 \pm 1\%$ and $23 \pm 1\%$, respectively, at the MSA level. Mean daily population-weighted NO_2 TVCDs for Asians equal those for non-Hispanic/Latino whites within the UA but are $9 \pm 1\%$ higher across the MSA, mainly due to the inclusion of the large Asian population around Sugar Land in southwest Houston (Figure 1d). We observe larger inequalities at the MSA level, reflecting intraurban NO_2 differences.^{3,94} UA and MSA-level relative ($r = 0.83$ – 0.92) and absolute ($r = 0.88$ – 0.95) inequalities are strongly correlated (Figure S3). Errors for mean inequalities are 95% confidence intervals, which we derive from bootstrapped distributions sampled with replacement 10^4 times. Absolute census tract-scale NO_2 inequalities are often lower than the precision of individual TROPOMI NO_2 TVCDs, which have a median daily pixel-level precision of $9.9 \times 10^{14} \text{ molecules cm}^{-2}$ (approximately 30% of mean NO_2 TVCDs) over May 2018–November 2022 in the Houston UA. However, this imprecision improves through spatial and temporal averaging,⁹⁵ done here through population weighting over all census tracts in the UA or MSA and by reporting daily inequality results as means over many days. Sampling and nonsampling (e.g., measurement, coverage, nonresponse, and processing errors) errors in the ACS influence the accuracy and precision of tract-scale NO_2 inequalities as well and, when random, also improve through averaging to higher geographic levels.

We report NO_2 inequalities during 27 TRACER-AQ flights using GCAS separately in the late morning, midday, and afternoon (Table 2). Relative inequalities are not statistically significantly different with time of daytime, although there may be a tendency toward lower relative inequalities at midday. Absolute NO_2 inequalities are significantly higher in the morning than midday and afternoon, and there are multiple factors that could influence these differences. While wind speeds are similar on average during all flights, the atmosphere

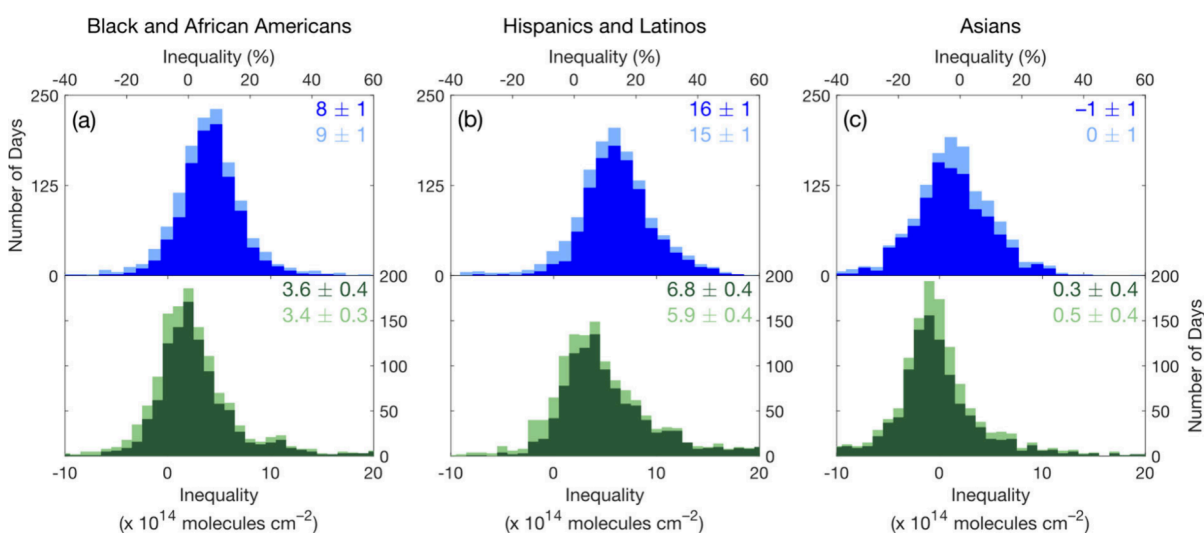


Figure 5. Daily UA-level TROPOMI NO₂ inequalities (May 2018–November 2022). Relative (%) and absolute (molecules cm⁻²) inequalities on all days (light blue and light green, respectively) and on days meeting metric-specific coverage thresholds (bright blue and dark green, respectively) for Black and African Americans (a), Hispanics and Latinos (b), and Asians (c). Bootstrap mean inequalities, sampled with replacement 10⁴ times, are reported with uncertainties as 95% confidence intervals.

Table 2. Relative and Absolute Mean GCAS NO₂ Inequalities in the Houston MSA During TRACER-AQ in the Morning (9–11:30 am LT), at Midday (11:30 am–2 pm LT), and in the Afternoon (2:30–5 pm LT); Relative and Absolute Mean Daily TROPOMI NO₂ Inequalities (May 2018–November 2022) along a Representative TRACER-AQ Flight Raster (Afternoon, 25 September 2021); and GCAS Inequalities along Spatially Coincident TRACER-AQ and DISCOVER-AQ Tracts during TRACER-AQ (2021) and DISCOVER-AQ (2013)^a

| | GCAS TRACER-AQ morning | GCAS TRACER-AQ midday | GCAS TRACER-AQ afternoon | TROPOMI along TRACER-AQ raster | 2021 GCAS (TRACER-AQ) | 2013 GCAS (DISCOVER-AQ) |
|--|------------------------|-----------------------|--------------------------|--------------------------------|-----------------------|-------------------------|
| Relative Inequalities (%) | | | | | | |
| Black and African Americans | 17 ± 7 | 12 ± 6 | 13 ± 4 | 13 ± 1 | 9 ± 8 | 10 ± 6 |
| Hispanics and Latinos | 27 ± 4 | 20 ± 6 | 25 ± 2 | 22 ± 1 | 24 ± 6 | 20 ± 5 |
| Asians | 12 ± 10 | 13 ± 10 | 11 ± 4 | 3 ± 2 | 9 ± 6 | 11 ± 4 |
| Absolute Inequalities (x 10 ¹⁴ molecules cm ⁻²) | | | | | | |
| Black and African Americans | 14.4 ± 5.8 | 6.8 ± 3.9 | 8.2 ± 2.6 | 6.0 ± 0.7 | 4.9 ± 4.6 | 10.9 ± 6.3 |
| Hispanics and Latinos | 22.7 ± 4.4 | 11.9 ± 3.4 | 16.0 ± 3.6 | 10.6 ± 1.0 | 16.4 ± 3.7 | 19.3 ± 5.9 |
| Asians | 17.0 ± 12.9 | 9.2 ± 6.9 | 7.6 ± 3.8 | 2.5 ± 1.0 | 9.6 ± 6.2 | 9.4 ± 3.7 |

^aAirborne and TROPOMI uncertainties are 95% confidence intervals of bootstrap mean inequalities, sampled with replacement 10⁴ times.

is typically more stable in morning than at midday, affecting the NO₂ distribution in the nearfield of NO_x sources,¹⁹ with convective mixing common in the afternoon in Houston. The surface mixed layer height is typically shallower in the morning than afternoon; however, this will have a larger effect on surface concentrations than TVCDs. We also expect higher rush hour NO_x emissions and longer NO₂ chemical lifetimes⁹⁶ in the morning and late afternoon compared to midday. Diurnal variability in absolute inequalities has implications for interpreting observations from TROPOMI, which collects measurements at 12–3 pm LT over Houston, and the recently-launched TEMPO (Tropospheric Emissions: Monitoring of Pollution) instrument, which scans North America hourly during daylight hours from onboard a geostationary satellite.⁹⁷ Our analysis in the New York City–Newark UA found fewer statistically significant morning–afternoon differences in absolute NO₂ inequalities,⁴¹ suggesting there is more to learn from TEMPO concerning temporal variability in the NO₂ distribution. Because GCAS subsampled the MSA, we also

report mean daily TROPOMI NO₂ inequalities (May 2018–November 2022) along a representative TRACER-AQ flight for comparison (Table 2).

GCAS NO₂ measurements in Houston collected during TRACER-AQ and DISCOVER-AQ offer observational insight into trends from 2013 to 2021 (Table 2). We compare weekday population-weighted, tract-average NO₂ columns in spatially coincident census tracts along representative TRACER-AQ and DISCOVER-AQ flight patterns (SI Appendix 1; Figure S4; Tables S8–S11). We calculate inequalities using the 2020 ACS for both DISCOVER-AQ and TRACER-AQ to allow comparisons across the same tracts and isolate effects of changes in NO₂ concentrations from demographics. We find relative NO₂ inequalities are statistically indistinguishable, with overlapping 95% confidence intervals for NO₂ inequalities in 2013 and 2021 and by the Wilcoxon rank sum test, a non-parametric two-sample t-test. While absolute inequalities were always lower during TRACER-AQ than DISCOVER-AQ, they were variable day to day, in addition to the relatively small

number of aircraft observations, such that we lack the precision on their means (not the observations themselves) to interpret the differences. UA-wide mean NO_2^* mixing ratios were slightly higher and more variable during DISCOVER-AQ (6.7 ± 6.2 ppb) than TRACER-AQ flights (6.0 ± 4.3 ppb); winds were slower during TRACER-AQ (2.1 ± 0.8 m s^{-1}) than DISCOVER-AQ (3.1 ± 1.2 m s^{-1}). Slower mean winds during TRACER-AQ may have worsened inequalities, while lower NO_2^* corresponds to lower absolute inequalities (discussed below). Previous work has shown downward NO_x emissions trends have not reduced relative NO_2 inequalities in U.S. cities using NO_2 empirical models;^{12,88} however, this has not yet been demonstrated with observations directly to our knowledge.

Relationships between daily UA-level census tract-scale TROPOMI NO_2 inequalities, surface winds, and overall NO_2 pollution (Table 3; Figures S5–S7) underscore the need for

Table 3. Spearman Rank Correlation Coefficients (2018–2022) with $p < 0.050$ in Winter and O_3 Season: Daily Absolute TROPOMI Inequalities and Daytime (12–3 pm LT) Surface Wind Speed, NO_2^* Mixing Ratios, and Daily UA-Level TROPOMI NO_2 TVCDs and Daily Relative TROPOMI Inequalities and Daytime NO_2^* Mixing Ratios and UA-Level TROPOMI NO_2 TVCDs

| | Absolute Inequality Correlations | | | Relative Inequality Correlations | |
|-----------------------------|--------------------------------------|-------------------------|---------------------|----------------------------------|---------------------|
| | Wind Speed | Surface NO_2^* | NO_2 TVCDs | Surface NO_2^* | NO_2 TVCDs |
| | Winter (December–February) | | | | |
| Black and African Americans | −0.40 | 0.44 | 0.55 | 0.25 | 0.26 |
| Hispanics and Latinos | −0.62 | 0.67 | 0.67 | 0.31 | 0.17 |
| Asians | | | 0.21 | | 0.21 |
| | O_3 Season (March–November) | | | | |
| Black and African Americans | −0.34 | 0.48 | 0.65 | 0.17 | 0.20 |
| Hispanics and Latinos | −0.51 | 0.61 | 0.77 | 0.24 | 0.26 |
| Asians | −0.17 | | 0.15 | | 0.07 |

locally targeted controls over sector-based approaches to reducing NO_2 disparities. Absolute NO_2 inequalities are moderately negatively associated with wind speeds for most groups, as faster winds distribute NO_2 away from NO_x sources, showing NO_2 inequalities arise from the distribution of NO_x sources, as well as that daily NO_2 inequalities vary meaningfully with relevant atmospheric conditions. Absolute NO_2 inequalities moderately correlate with UA-mean surface NO_2^* and NO_2 TVCDs in the winter and during O_3 season for most metrics. At the same time, relative inequalities are more weakly associated with overall NO_2 . Differences in these correlations for absolute and relative NO_2 inequalities manifest from NO_x sources being systematically located in Black and African American and Hispanic and Latino, as NO_2 concentrations in the nearfield of emitters are more temporally variable than the physical locations of NO_x sources. As a consequence, emissions reductions that maintain unequal source distributions, such as sector-based approaches, lower overall NO_2 pollution and absolute differences between groups but have little effect on relative inequalities, which require location-specific policy interventions.⁹⁸

NO_2 Inequalities and O_3 Air Quality. We use daily observations of NO_2 inequalities to investigate relationships between neighborhood-level NO_2 distributions and O_3 air quality. First, applying an established approach to understanding the influence of meteorology on O_3 variability in Houston, we disaggregate observations by winds using principal component and cluster analysis,^{48,53,99–103} presenting cluster characteristics that include census tract-scale NO_2 inequalities. We generate one two-dimensional principal component for mean daytime (12–3 pm LT) u and v resultant winds during O_3 season, which captures 88% of the observed variability in u and v components. We then apply k -means clustering with 1,000 iterations to generate eight wind clusters, with the first centroid selected at random, from the iteration with the lowest total sum of distances (Figure 6; Table 4). We selected the optimal number of clusters, allowed to range 1–10, using the Calinski-Harabasz criterion, maximizing the ratio of the between-cluster variance to the within-cluster variance with respect to the number of clusters.¹⁰⁴ We confirmed the identified number of clusters using the elbow method with 10^3 iterations, with the optimal number of clusters based on the variance explained.¹⁰⁵ Eight clusters balanced clarity and complexity relevant to relationships between NO_2 inequalities and MDA8 O_3 . Missing daytime winds are filled using measurements from the closest proximity monitor with observations. We renamed the clusters 1–8 from most to least frequent MDA8 O_3 NAAQS exceedances. The analysis reproduces results in the literature, with high O_3 days associated with easterly and east-southeasterly winds.^{48,53,100,103} Figure 6 highlights the variability in NO_2 spatial distributions lost through averaging (Figure 1c), with results based on long-term or annual averages representing conditions that infrequently occur.

MDA8 O_3 NAAQS exceedances are most frequent in cluster 1, when winds are on average slow and easterly—corresponding to the largest absolute daily TROPOMI race-ethnicity inequalities (Table 4). Cluster 1 is the primary wind condition in which we observe statistically significant UA-level inequalities for Asians, with NO_2 from the Ship Channel transported toward Sugar Land in southwest Houston and stagnant NO_x emissions around the nearby coal-fired W.A. Parrish Generating Station. This explains why NO_2 inequalities for Asians are not strongly correlated with wind speed or overall NO_2 pollution level (Table 3). MDA8 O_3 NAAQS exceedances are also common in clusters 2–4, when winds are slow (~ 1.6 m s^{-1}) and east-southeasterly, southerly, and westerly, with elevated UA-level absolute daily TROPOMI NO_2 inequalities for all groups except Asians. Clusters 5–8 include the fewest number of O_3 NAAQS exceedances, occurring on <5% of days. These clusters are characterized by faster winds, lower UA-mean NO_2^* , and lower absolute tract-scale daily TROPOMI NO_2 inequalities. Wind conditions have less influence on relative NO_2 inequalities, as winds do not affect the locations of NO_x sources. Observed correspondence between MDA8 O_3 and absolute census tract-scale NO_2 inequalities indicates similar atmospheric conditions exacerbate both phenomena and/or high O_3 and NO_2 inequalities are linked chemically.

PO_3 varies nonlinearly with NO_2 concentrations (Figure 7a); therefore, NO_2 inequalities and city-wide O_3 air quality are potentially coupled chemically. Briefly, PO_3 increases with increasing NO_x when NO is the limiting reagent in O_3 -forming radical cycling (PO_3 chemistry is NO_x limited). PO_3 decreases

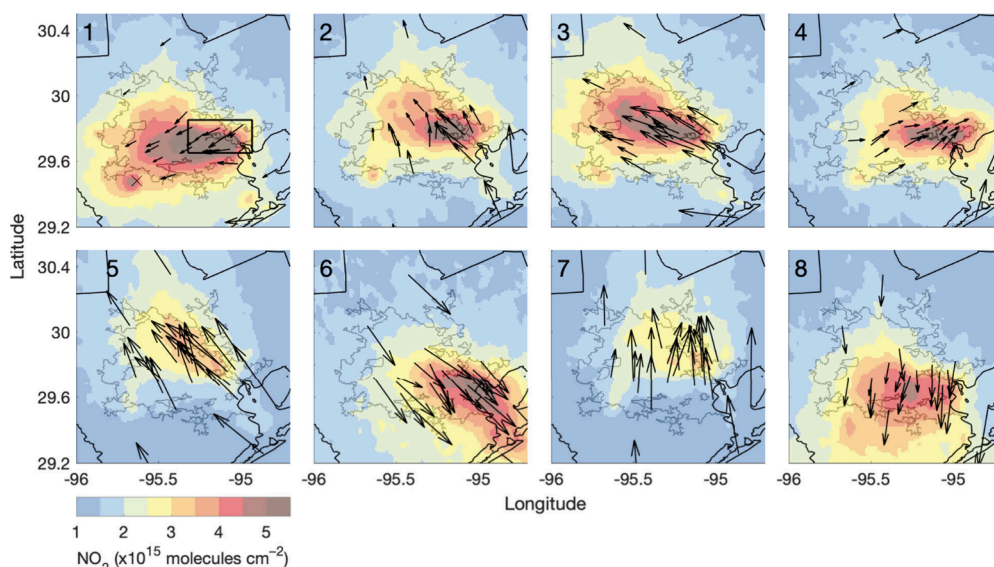


Figure 6. Distinct mean daytime (12–3 pm LT) wind clusters during O₃ season (March–November) over May 2018–November 2022 in the Houston MSA and corresponding TROPOMI NO₂ TVCDs oversampled to 0.01° × 0.01°. Wind vector length is proportional to wind speed, with mean wind speeds given in Table 4. The W.A. Parrish Generating Station is indicated with an × and the Houston Ship Channel with a thick black box in cluster 1. The thin inner gray and outer black lines are the UA and MSA boundaries, respectively.

Table 4. Mean Daytime Wind Cluster Characteristics: Number of Days in Each Cluster; MSA-Mean Wind Speed ($\pm 1\sigma$) and Direction; MSA-Level MDA8 O₃ NAAQS Exceedances, Both Number and Frequency; UA-Mean NO₂* ($\pm 1\sigma$); and Mean Daily TROPOMI Relative and Absolute Inequalities Based on Bootstrapped Distributions Sampled with Replacement 10⁴ Times with Uncertainties as 95% Confidence Intervals

| | Cluster | | | | | | | |
|---|--|------------|--------------------|------------|---------------|---------------|------------|---------------|
| | 1 | 2 | 3 | 4 | 5 | 6 | 7 | 8 |
| Number of days | 186 | 279 | 193 | 112 | 170 | 48 | 162 | 136 |
| Wind speed (m s ⁻¹) | 0.7 | 1.2 | 2.2 | 1.3 | 3.7 | 4.2 | 3.5 | 2.5 |
| Wind direction | easterly | southerly | east southeasterly | westerly | southeasterly | northwesterly | southerly | northwesterly |
| Temperature (°C) | 28 | 32 | 27 | 30 | 28 | 23 | 30 | 23 |
| O ₃ NAAQS exceedances | 49 | 38 | 22 | 12 | 9 | 2 | 5 | 4 |
| O ₃ exceedance frequency (%) | 26 | 14 | 11 | 11 | 5 | 4 | 3 | 3 |
| NO ₂ * (ppb) | 7.4 | 6.6 | 7.2 | 6.1 | 5.1 | 5.5 | 3.9 | 6.7 |
| | UA | | | | | | | |
| | Mean Daily Relative Inequalities (%) | | | | | | | |
| Black and African Americans | 11 ± 1 | 13 ± 1 | 10 ± 2 | 9 ± 3 | 9 ± 2 | -3 ± 3 | 10 ± 1 | 6 ± 2 |
| Hispanics and Latinos | 19 ± 2 | 22 ± 2 | 17 ± 2 | 18 ± 6 | 14 ± 2 | 14 ± 3 | 13 ± 2 | 9 ± 2 |
| Asians | 9 ± 2 | 0 ± 1 | -1 ± 2 | -6 ± 2 | -3 ± 2 | -15 ± 4 | -0 ± 1 | 4 ± 2 |
| | Mean Daily Absolute Inequalities (×10 ¹⁴ molecules cm ⁻²) | | | | | | | |
| Black and African Americans | 5.9 ± 1.1 | 5.0 ± 0.8 | 3.7 ± 0.6 | 3.3 ± 0.9 | 2.3 ± 0.6 | -0.7 ± 0.5 | 2.1 ± 0.3 | 2.1 ± 0.5 |
| Hispanics and Latinos | 9.5 ± 1.4 | 9.1 ± 1.4 | 6.9 ± 0.8 | 8.1 ± 1.5 | 3.7 ± 0.6 | 4.1 ± 0.8 | 2.9 ± 0.4 | 2.9 ± 0.5 |
| Asians | 5.3 ± 1.5 | -0.1 ± 0.5 | -0.4 ± 1.0 | -0.9 ± 1.4 | -0.7 ± 0.4 | -3.1 ± 0.5 | -0.0 ± 0.3 | 1.8 ± 0.7 |

with increasing NO_x when NO₂ predominately combines with OH to produce nitric acid, reducing O₃-forming reactions between OH and VOCs (PO₃ is NO_x suppressed). This nonlinear chemistry has important regulatory consequences, as NO_x decreases improve O₃ air quality when chemistry is NO_x limited, while the same reductions worsen NO_x-suppressed O₃. When PO₃ dominates the O₃ mass balance, MDA8 O₃ varies as the integral of PO₃ across the intraurban NO₂ heterogeneity, and, in Houston, NO_x-limited and suppressed conditions are both present.⁵⁶ Because PO₃ depends nonlinearly on NO₂, we describe O₃-season relationships between NO₂ inequalities and the highest daily MSA-level MDA8 O₃ using a generalized additive model (GAM), a regression approach previously

applied to nonlinear systems, including O₃.^{106–110} PO₃ also depends nonlinearly on VOC reactivity to OH, defined as the sum of the product of VOC concentrations and their bimolecular reaction rate with OH.¹¹¹ Temperature is a proxy for VOC-OH reactivity where a major portion of VOC emissions are temperature dependent, verifiable through the observed O₃-NO₂ dependence under different temperatures.¹¹² To consider VOC-OH reactivity, we apply the GAM separately under low (<25°C), moderate (25–28°C), and high (>28°C) daytime mean temperatures conditions. Results informing GAM selection and evaluation are available in the Supporting Information (SI Appendix 2; Tables S12–13; Figures S8–S16).

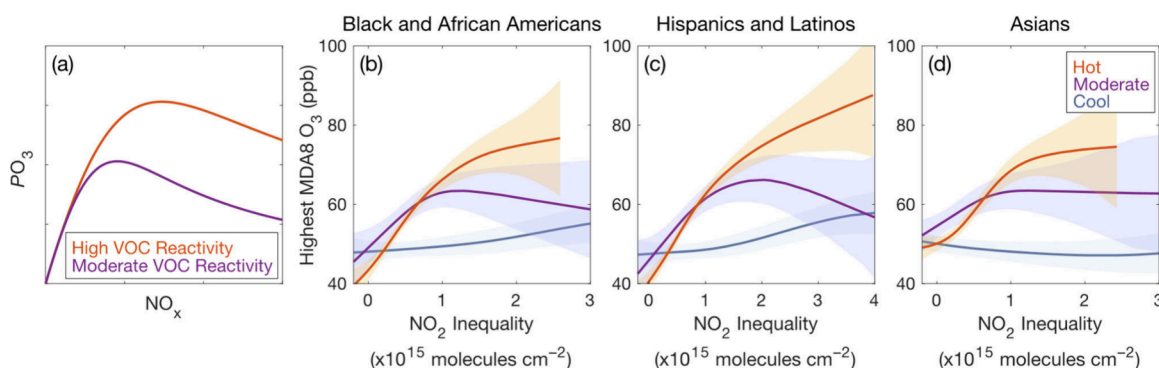


Figure 7. Analytical model demonstrating relationships between PO_3 , NO_x , and VOC-OH reactivity (a). GAMs of daily MSA-level absolute TROPOMI NO_2 inequalities (molecules cm^{-2}) versus highest daily MDA8 O_3 (ppb) during O_3 -season (March–November 2018–2022) on days meeting coverage thresholds under moderate (purple) and high (orange) daily maximum temperatures for Black and African Americans (b), Hispanics and Latinos (c), and Asians (d). Envelopes are 95% confidence intervals.

GAMs of MDA8 O_3 versus NO_2 inequalities reproduce the nonlinear dependence of PO_3 on NO_2 concentrations (Figure 7). The highest MDA8 O_3 occur hot days, i.e., under higher VOC-OH reactivity conditions, and when absolute NO_2 inequalities are large. We observe lower MDA8 O_3 when temperatures are moderate (lower VOC-OH reactivity) and NO_2 inequalities are large, with similar MDA8 O_3 to hot days when NO_2 is more evenly distributed (PO_3 is NO_x limited). At low temperatures, relationships between MDA8 O_3 and NO_2 inequalities suggest a more limited role for PO_3 on MDA8 O_3 . A key observation is that the transition between NO_x -limited and NO_x -suppressed PO_3 chemistry that is near peak MDA8 O_3 occurs at higher absolute NO_2 inequalities under higher temperature conditions, consistent with hotter temperatures corresponding to higher VOC-OH reactivities, which in turn require more NO_2 to drive nitric acid production.¹¹² While at very high NO concentrations O_3 can be titrated to NO_2 , O_3 titration does not have the same functional form as PO_3 with VOC-OH reactivity versus NO_2 .

The GAMs demonstrate that NO_2 inequalities affect PO_3 chemistry and not merely that MDA8 O_3 and NO_2 inequalities covary under certain atmospheric conditions. We note, it is not the inequalities per se, but the unequal NO_2 distributions resulting from NO_x sources being disproportionately located in a subset of neighborhoods that drives PO_3 . That said, NO_x emission sources overburden communities of color because of environmental racism in historical and contemporary decision-making. Past research has already shown that PO_3 chemistry is spatially heterogeneous within Houston,^{46,49,56,113,114} and, because PO_3 chemistry is nonlinear, it follows logically that the same NO_x emission reductions applied evenly across a city would be less effective than a series of localized controls responsive to specific PO_3 mechanisms (NO_x limited versus NO_x suppressed) as they vary in space. Wang et al.⁵⁸ used the adjoint of the Community Multiscale Air Quality model focused on California to determine that PO_3 is disproportionately sensitive to spatially localized controls. Our work implies that NO_x emissions controls that eliminate neighborhood-level NO_2 inequalities will have O_3 air quality co-benefits, with regulatory decision-making consolidating NO_x sources in a subset of Houston neighborhoods hindering O_3 NAAQS compliance. While MDA8 O_3 is largely NO_x limited with respect to NO_2 inequalities on high temperature days, MDA8 O_3 is more NO_x suppressed as a function of NO_2 inequalities when temperatures are moderate, meaning even steeper NO_x

reductions that also have the effect of decreasing NO_2 inequalities are required to lower O_3 under these conditions. Based on observed differences in correlations between absolute and relative NO_2 inequalities with overall NO_2 (Table 3), decreases in NO_2 inequalities, and hence MDA8 O_3 , require locally targeted NO_x reductions in neighborhoods where residents are primarily Black, Latinx, and Asian.

Implications. In Houston, daily TROPOMI NO_2 TVCDs capture a major portion of census tract-scale NO_2 inequalities compared to spatiotemporally coincident GCAS measurements that resolve length scales of dispersion. Mean daily TROPOMI NO_2 inequalities are insensitive to TROPOMI pixel size after the initial information loss with respect to GCAS. In Houston, and other U.S. cities, communities of color are statistically overburdened by air pollution sources,^{98,115,116} including NO_x sources.¹⁶ This is a consequence of historical (e.g., redlining) and contemporary (e.g., permitting) decision-making that clusters emission sources in a subset of city neighborhoods, creating source regions such as the Houston Ship Channel, in combination with historical and contemporary policies and practices causing and reinforcing housing segregation,¹ including white violence, housing discrimination, and separating communities with freeways.^{117–121} When NO_x sources are in close proximity, their individual pollutant decay gradients also spatially aggregate; as a result, a major portion of inequalities persist over spatial scales greater than length scales of dispersion, the physical process motivating the application of very-high spatial resolution models and measurements. Fine-scale observations are therefore not always required as evidence of air pollution inequalities or to inform related policy making and accountability. While daily TVCDs are coarse (20–89 km^2), they retain a wider range of NO_2 values, especially in the high tail of the NO_2 distribution, which drive inequalities. Daily mean NO_2 TVCDs result in higher, and therefore more accurate, absolute NO_2 inequalities than oversampled TVCDs ($0.01^\circ \times 0.01^\circ$), as TROPOMI pixels and oversampling grids are large relative to the scale of dispersion. This has relevance to future work based on TEMPO observations, which are not anticipated to meet the pixel overlap requirements for oversampling.

We find that neighborhood-level NO_2 inequalities and city-wide O_3 are coupled air quality issues in Houston. GAMs relating NO_2 inequalities and MDA8 O_3 under different temperature conditions reproduce established nonlinear relationships between PO_3 , NO_2 , and VOC-OH reactivity.

This has policy consequences, producing empirical evidence that MDA8 O₃ is sensitive to the spatial distribution of NO_x emissions reductions. O₃ control is typically approached through sector-based NO_x and VOC emissions reductions without also considering distributive inequalities in O₃ precursors.¹²² However, we find that targeted NO_x emissions reductions where NO_x sources are clustered—in communities of color—would lower both NO₂ inequalities and city-wide MDA8 O₃ in Houston, especially on hot days when MDA8 O₃ is highest. This means that permitting and other policies concentrating sources in a subset of Houston neighborhoods affect O₃ NAAQS attainment and calls for a reconceptualization of decision-making to include facility/emissions location.

While there is growing evidence that locally-targeted regulatory interventions are required to reduce and eliminate air pollution disparities,^{41,98} there are barriers to their adoption, as community-focused air quality plans and recommendations potentially cannot be pursued through policy making at any level.¹²³ Houston and Pasadena (which is in the Houston UA) are among the few major U.S. municipalities without formal zoning, an established tool for localities to influence their own land use, including air pollution source distribution, through the institution of bans, programs, and environmental review processes.¹²⁴ Additionally, Houston's efforts to address air quality concerns through the local ordinance process have been invalidated by the Texas Supreme Court,^{125,126} further limiting the city from regulating emissions from facilities permitted by the Texas Commission on Environmental Quality (TCEQ). TCEQ does not have an office or staff focused on environmental justice, chooses not to use that term (any relevant activities are instead described as Title VI compliance), and continues to issue permits without considering cumulative impacts, including facility clustering. However, TCEQ does have a commitment to O₃ compliance,¹²⁷ making this a politically available pathway for addressing inequality in absence of other approaches. Here, we demonstrate that MDA8 O₃ varies as a function of these neighborhood-level NO₂ inequalities, with locally-targeted NO_x emissions controls required to address NO₂ disparities and having substantial O₃ air quality co-benefits. This conclusion has policy relevance as the state has the authority, resources, and initiative to meet the O₃ NAAQS and is also evidence that TCEQ must contend with practices and policies of environmental racism to improve O₃ air quality.

■ ASSOCIATED CONTENT

SI Supporting Information

The Supporting Information is available free of charge at <https://pubs.acs.org/doi/10.1021/acsestair.4c00009>.

Surface wind roses corresponding to Figure 1, surface monitor locations, detailed TRACER-AQ inequality results, population weighting equation, TROPOMI inequalities as a function of observation coverage and pixel area, comparison of oversampled and time-averaged inequalities by S-SP orbit, mean daily TROPOMI population-weighted NO₂, correlations between daily UA and MSA-level inequalities, details for the comparison between DISCOVER-AQ and TRACER-AQ inequalities, scatterplots of NO₂ inequalities versus surface winds and NO₂*, and technical details on generalized additive model (GAM) con-

struction, including comparisons of GAM methods (PDF)

■ AUTHOR INFORMATION

Corresponding Author

Sally E. Pusede — Department of Environmental Sciences, University of Virginia, Charlottesville, Virginia 22904, United States; orcid.org/0000-0002-3041-0209; Email: sepusede@virginia.edu

Authors

Isabella M. Dressel — Department of Environmental Sciences, University of Virginia, Charlottesville, Virginia 22904, United States; orcid.org/0000-0002-3796-0641

Sixuan Zhang — Department of Environmental Sciences, University of Virginia, Charlottesville, Virginia 22904, United States

Mary Angelique G. Demetillo — Department of Environmental Sciences, University of Virginia, Charlottesville, Virginia 22904, United States; NASA Langley Research Center, Hampton, Virginia 23681, United States; orcid.org/0000-0002-0618-9022

Shan Yu — Department of Statistics, University of Virginia, Charlottesville, Virginia 22904, United States

Kimberly Fields — Carter G. Woodson Institute for African American and African Studies, University of Virginia, Charlottesville, Virginia 22904, United States

Laura M. Judd — NASA Langley Research Center, Hampton, Virginia 23681, United States

Caroline R. Nowlan — Atomic and Molecular Physics Division, Center for Astrophysics | Harvard & Smithsonian, Cambridge, Massachusetts 02138, United States; orcid.org/0000-0002-8718-9752

Kang Sun — Department of Civil, Structural and Environmental Engineering and Research and Education in eNergy, Environment and Water (RENEW) Institute, University at Buffalo, Buffalo, New York 14260, United States; orcid.org/0000-0002-9930-7509

Alexander Kotsakis — NASA Goddard Space Flight Center, Greenbelt, Maryland 20771, United States

Alexander J. Turner — Department of Atmospheric Sciences, University of Washington, Seattle, Washington 98195, United States

Complete contact information is available at: <https://pubs.acs.org/10.1021/acsestair.4c00009>

Notes

The authors declare no competing financial interest.

■ ACKNOWLEDGMENTS

This work was funded by the NASA New Investigator Program in Earth Science (80NSSC21K0935) and an NSF CAREER (AGS 2047150) awards to S.E.P. The University of Virginia (UVA) Karsh Institute of Democracy provided support through the UVA Repair Lab to S.E.P. and K.F. I.M.D. received funds from the Virginia Space Grant Consortium and M.A.G.D. from the NASA FINESST program (80NSSC20K1655). UVA Research Computing provided computational resources (rc.virginia.edu). We thank the TRACER-AQ science team and pilots and crew of the NASA JSC GV. TRACER-AQ data are publicly available (www-air.larc.nasa.gov/cgi-bin/ArcView/traceraq.2021).

TROPOMI Level 2 NO₂ TVCDs are accessible from the S-5P Pre-Ops Hub (scihub.copernicus.eu/). We acknowledge use of the U.S. Census database through the IPUMS National Historical Geographic Information System (nhgis.org)¹²⁸ and TIGER/Line shapefiles of Texas census tract polygons and UA and MSA boundaries from the Data.gov library (census.gov/cgi-bin/geo/shapefiles/index.php). NO₂*, MDA8 O₃, and wind speed, wind direction, and temperature datasets were downloaded via the U.S. EPA Air Quality System (aq5.epa.gov/aqsweb/documents/data_api.html).

REFERENCES

- (1) Bullard, R. *Dumping in Dixie: Race, Class, and Environmental Quality*; Westview Press: Boulder, CO, 1990.
- (2) Li, Z.; Konisky, D. M.; Ziogiannis, N. Racial, ethnic, and income disparities in air pollution: A study of excess emissions in Texas. *PLoS One* **2019**, *14* (8), No. e0220696.
- (3) Demetillo, M. A. G.; Navarro, A.; Knowles, K. K.; Fields, K. P.; Geddes, J. A.; Nowlan, C. R.; Janz, S. J.; Judd, L. M.; Al-Saadi, J.; Sun, K.; McDonald, B. C.; Diskin, G. S.; Pusede, S. E. Observing Nitrogen Dioxide Air Pollution Inequality Using High-Spatial-Resolution Remote Sensing Measurements in Houston, Texas. *Environmental Science & Technology* **2020**, *54* (16), 9882–9895.
- (4) Bullard, R. D. *Invisible Houston: The Black Experience in Boom and Bust*; Texas A & M University Press: College Station, 1987.
- (5) Collins, T. W.; Grineski, S. E.; Chakraborty, J.; Montgomery, M. C.; Hernandez, M. Downscaling Environmental Justice Analysis: Determinants of Household-Level Hazardous Air Pollutant Exposure in Greater Houston. *Annals of the Association of American Geographers* **2015**, *105* (4), 684–703.
- (6) Linder, S. H.; Marko, D.; Sexton, K. Cumulative Cancer Risk from Air Pollution in Houston: Disparities in Risk Burden and Social Disadvantage. *Environmental Science & Technology* **2008**, *42* (12), 4312–4322.
- (7) Hernandez, M.; Collins, T. W.; Grineski, S. E. Immigration, mobility, and environmental injustice: A comparative study of Hispanic people's residential decision-making and exposure to hazardous air pollutants in Greater Houston, Texas. *Geoforum* **2015**, *60*, 83–94.
- (8) Sansom, G.; Parras, J.; Parras, A.; Nieto, Y.; Arellano, Y.; Berke, P.; McDonald, T.; Shipp, E.; Horney, J. A. The Impacts of Exposure to Environmental Risk on Physical and Mental Health in a Small Geographic Community in Houston, TX. *Journal of Community Health* **2017**, *42* (4), 813–818.
- (9) Miller, D. J.; Actkinson, B.; Padilla, L.; Griffin, R. J.; Moore, K.; Lewis, P. G. T.; Gardner-Frolick, R.; Craft, E.; Portier, C. J.; Hamburg, S. P.; Alvarez, R. A. Characterizing Elevated Urban Air Pollutant Spatial Patterns with Mobile Monitoring in Houston, Texas. *Environmental Science & Technology* **2020**, *54* (4), 2133–2142.
- (10) American Lung Association. *State of the Air 2023 Report*; American Lung Association, 2023.
- (11) Apte, J. S.; Messier, K. P.; Gani, S.; Brauer, M.; Kirchstetter, T. W.; Lunden, M. M.; Marshall, J. D.; Portier, C. J.; Vermeulen, R. C. H.; Hamburg, S. P. High-Resolution Air Pollution Mapping with Google Street View Cars: Exploiting Big Data. *Environmental Science & Technology* **2017**, *51* (12), 6999–7008.
- (12) Liu, J.; Clark, L. P.; Bechle, M. J.; Hajat, A.; Kim, S.-Y.; Robinson, A. L.; Sheppard, L.; Szpiro, A. A.; Marshall, J. D. Disparities in Air Pollution Exposure in the United States by Race/Ethnicity and Income, 1990–2010. *Environmental Health Perspectives* **2021**, *129* (12), No. 127005.
- (13) Messier, K. P.; Chambliss, S. E.; Gani, S.; Alvarez, R.; Brauer, M.; Choi, J. J.; Hamburg, S. P.; Kerckhoffs, J.; LaFranchi, B.; Lunden, M. M.; Marshall, J. D.; Portier, C. J.; Roy, A.; Szpiro, A. A.; Vermeulen, R. C. H.; Apte, J. S. Mapping Air Pollution with Google Street View Cars: Efficient Approaches with Mobile Monitoring and Land Use Regression. *Environmental Science & Technology* **2018**, *52* (1), 12563–12572.
- (14) Tessum, C. W.; Hill, J. D.; Marshall, J. D. InMAP: A model for air pollution interventions. *PLoS One* **2017**, *12* (4), No. e0176131.
- (15) Di, Q.; Wang, Y.; Zanobetti, A.; Wang, Y.; Koutrakis, P.; Choirat, C.; Dominici, F.; Schwartz, J. D. Air Pollution and Mortality in the Medicare Population. *New England Journal of Medicine* **2017**, *376* (26), 2513–2522.
- (16) Demetillo, M. A. G.; Harkins, C.; McDonald, B. C.; Chodrow, P. S.; Sun, K.; Pusede, S. E. Space-Based Observational Constraints on NO₂ Air Pollution Inequality From Diesel Traffic in Major US Cities. *Geophysical Research Letters* **2021**, *48* (17), No. e2021GL094333.
- (17) Wang, Y.; Liu, P.; Schwartz, J.; Castro, E.; Wang, W.; Chang, H.; Scovronick, N.; Shi, L. Disparities in ambient nitrogen dioxide pollution in the United States. *Proceedings of the National Academy of Sciences U. S. A.* **2023**, *120* (16), No. e2208450120.
- (18) Clark, L. P.; Millet, D. B.; Marshall, J. D. National Patterns in Environmental Injustice and Inequality: Outdoor NO₂ Air Pollution in the United States. *PLoS One* **2014**, *9* (4), No. e94431.
- (19) Choi, W.; He, M. L.; Barbesant, V.; Kozawa, K. H.; Mara, S.; Winer, A. M.; Paulson, S. E. Prevalence of wide area impacts downwind of freeways under pre-sunrise stable atmospheric conditions. *Atmospheric Environment* **2012**, *62*, 318–327.
- (20) Karner, A. A.; Eisinger, D. S.; Niemeier, D. A. Near-Roadway Air Quality: Synthesizing the Findings from Real-World Data. *Environmental Science & Technology* **2010**, *44* (14), 5334–5344.
- (21) Harkins, C.; McDonald, B. C.; Henze, D. K.; Wiedinmyer, C. A fuel-based method for updating mobile source emissions during the COVID-19 pandemic. *Environmental Research Letters* **2021**, *16*, No. 065018.
- (22) Travis, K. R.; Jacob, D. J.; Fisher, J. A.; Kim, P. S.; Marais, E. A.; Zhu, L.; Yu, K.; Miller, C. C.; Yantosca, R. M.; Sulprizio, M. P.; Thompson, A. M.; Wennberg, P. O.; Crouse, J. D.; St. Clair, J. M.; Cohen, R. C.; Laughner, J. L.; Dibb, J. E.; Hall, S. R.; Ullmann, K.; Wolfe, G. M.; Pollack, I. B.; Peischl, J.; Neuman, J. A.; Zhou, X. Why do models overestimate surface ozone in the Southeast United States? *Atmospheric Chemistry and Physics* **2016**, *16* (21), 13561–13577.
- (23) Yu, K. A.; McDonald, B. C.; Harley, R. A. Evaluation of Nitrogen Oxide Emission Inventories and Trends for On-Road Gasoline and Diesel Vehicles. *Environmental Science & Technology* **2021**, *55* (10), 6655–6664.
- (24) Kim, S. W.; McKeen, S. A.; Frost, G. J.; Lee, S. H.; Trainer, M.; Richter, A.; Angevine, W. M.; Atlas, E.; Bianco, L.; Boersma, K. F.; Brioude, J.; Burrows, J. P.; de Gouw, J.; Fried, A.; Gleason, J.; Hilboll, A.; Mellqvist, J.; Peischl, J.; Richter, D.; Rivera, C.; Ryerson, T.; te Lintel Hekkert, S.; Walega, J.; Warneke, C.; Weibring, P.; Williams, E. Evaluations of NO_x and highly reactive VOC emission inventories in Texas and their implications for ozone plume simulations during the Texas Air Quality Study 2006. *Atmospheric Chemistry and Physics* **2011**, *11* (22), 11361–11386.
- (25) Rivera, C.; Mellqvist, J.; Samuelsson, J.; Lefer, B.; Alvarez, S.; Patel, M. R. Quantification of NO₂ and SO₂ emissions from the Houston Ship Channel and Texas City industrial areas during the 2006 Texas Air Quality Study. *Journal of Geophysical Research: Atmospheres* **2010**, *115*, No. D08301.
- (26) Washenfelder, R. A.; Trainer, M.; Frost, G. J.; Ryerson, T. B.; Atlas, E. L.; de Gouw, J. A.; Flocke, F. M.; Fried, A.; Holloway, J. S.; Parrish, D. D.; Peischl, J.; Richter, D.; Schaffler, S. M.; Walega, J. G.; Warneke, C.; Weibring, P.; Zheng, W. Characterization of NO_x, SO₂, ethene, and propene from industrial emission sources in Houston, Texas. *Journal of Geophysical Research: Atmospheres* **2010**, *115*, No. D16311.
- (27) Anenberg, S. C.; Henze, D. K.; Tinney, V.; Kinney, P. L.; Raich, W.; Fann, N.; Malley, C. S.; Roman, H.; Lamsal, L.; Duncan, B.; Martin, R. V.; van Donkelaar, A.; Brauer, M.; Doherty, R.; Jonson, J. E.; Davila, Y.; Sudo, K.; Kuylenstierna, J. C. I. Estimates of the Global Burden of Ambient PM_{2.5}, Ozone, and NO₂ on Asthma Incidence and Emergency Room Visits. *Environmental Health Perspectives* **2018**, *126* (10), No. 107004.
- (28) Southerland, V. A.; Anenberg, S. C.; Harris, M.; Apte, J.; Hystad, P.; van Donkelaar, A.; Martin, R. V.; Beyers, M.; Roy, A.

Assessing the Distribution of Air Pollution Health Risks within Cities: A Neighborhood-Scale Analysis Leveraging High-Resolution Data Sets in the Bay Area, California. *Environmental Health Perspectives* **2021**, *129* (3), No. 037006.

(29) Atkinson, R. W.; Butland, B. K.; Anderson, H. R.; Maynard, R. L. Long-term Concentrations of Nitrogen Dioxide and Mortality: A Meta-analysis of Cohort Studies. *Epidemiology* **2018**, *29* (4), 460–472.

(30) Brunekreef, B.; Holgate, S. T. Air pollution and health. *Lancet* **2002**, *360* (9341), 1233–1242.

(31) Burnett, R. T.; Stieb, D.; Brook, J. R.; Cakmak, S.; Dales, R.; Raizenne, M.; Vincent, R.; Dann, T. Associations between short-term changes in nitrogen dioxide and mortality in Canadian cities. *Archives of Environmental Health* **2004**, *59* (5), 228–236.

(32) Levy, I.; Mihele, C.; Lu, G.; Narayan, J.; Brook, J. R. Evaluating Multipollutant Exposure and Urban Air Quality: Pollutant Interrelationships, Neighborhood Variability, and Nitrogen Dioxide as a Proxy Pollutant. *Environmental Health Perspectives* **2014**, *122* (1), 65–72.

(33) Antonczak, B.; Thompson, T. M.; DePaola, M. W.; Rowangould, G. 2020 Near-roadway population census, traffic exposure and equity in the United States. *Transportation Research Part D: Transport and Environment* **2023**, *125*, No. 103965.

(34) Chodrow, P. S. Structure and information in spatial segregation. *Proceedings of the National Academy of Sciences U. S. A.* **2017**, *114* (44), 11591–11596.

(35) Adar, S. D.; Kaufman, J. D. Cardiovascular disease and air pollutants: Evaluating and improving epidemiological data implicating traffic exposure. *Inhalation Toxicology* **2007**, *19*, 135–149.

(36) Edwards, J.; Walters, S.; Griffiths, R. K. Hospital Admissions for Asthma in Preschool-Children – Relationship to Major Roads in Birmingham, United-Kingdom. *Archives of Environmental Health* **1994**, *49* (4), 223–227.

(37) Gauderman, W. J.; Avol, E.; Lurmann, F.; Kuenzli, N.; Gilliland, F.; Peters, J.; McConnell, R. Childhood asthma and exposure to traffic and nitrogen dioxide. *Epidemiology* **2005**, *16* (6), 737–743.

(38) Lin, S.; Munsie, J. P.; Hwang, S.-A.; Fitzgerald, E.; Cayo, M. R. Childhood Asthma Hospitalization and Residential Exposure to State Route Traffic. *Environmental Research* **2002**, *88* (2), 73–81.

(39) Lipfert, F. W.; Wyzga, R. E. On exposure and response relationships for health effects associated with exposure to vehicular traffic. *Journal of Exposure Science & Environmental Epidemiology* **2008**, *18* (6), 588–599.

(40) Wu, J.; Ren, C. Z.; Delfino, R. J.; Chung, J.; Wilhelm, M.; Ritz, B. Association between Local Traffic-Generated Air Pollution and Preeclampsia and Preterm Delivery in the South Coast Air Basin of California. *Environmental Health Perspectives* **2009**, *117* (11), 1773–1779.

(41) Dressel, I. M.; Demetillo, M. A. G.; Judd, L. M.; Janz, S. J.; Fields, K. P.; Sun, K.; Fiore, A. M.; McDonald, B. C.; Pusede, S. E. Daily Satellite Observations of Nitrogen Dioxide Air Pollution Inequality in New York City, New York and Newark, New Jersey: Evaluation and Application. *Environmental Science & Technology* **2022**, *56* (22), 15298–15311.

(42) Kerr, G. H.; Goldberg, D. L.; Anenberg, S. C. COVID-19 pandemic reveals persistent disparities in nitrogen dioxide pollution. *Proceedings of the National Academy of Sciences U. S. A.* **2021**, *118* (30), No. e2022409118.

(43) Kerr, G. H.; Goldberg, D. L.; Harris, M. H.; Henderson, B. H.; Hystad, P.; Roy, A.; Anenberg, S. C. Ethnoracial Disparities in Nitrogen Dioxide Pollution in the United States: Comparing Data Sets from Satellites, Models, and Monitors. *Environmental Science & Technology* **2023**, *57* (48), 19532–19544.

(44) Goldberg, D. L.; Tao, M.; Kerr, G. H.; Ma, S.; Tong, D. Q.; Fiore, A. M.; Dickens, A. F.; Adelman, Z. E.; Anenberg, S. C. Evaluating the spatial patterns of U.S. urban NO_x emissions using TROPOMI NO₂. *Remote Sensing of Environment* **2024**, *300*, No. 113917.

(45) Bradley, A. C.; Croes, B. E.; Harkins, C.; McDonald, B. C.; de Gouw, J. A. Air Pollution Inequality in the Denver Metroplex and its Relationship to Historical Redlining. *Environmental Science & Technology* **2024**, *58* (9), 4226–4236.

(46) Ryerson, T. B.; Trainer, M.; Angevine, W. M.; Brock, C. A.; Dissly, R. W.; Fehsenfeld, F. C.; Frost, G. J.; Goldan, P. D.; Holloway, J. S.; Hübler, G.; Jakoubek, R. O.; Kuster, W. C.; Neuman, J. A.; Nicks, D. K., Jr.; Parrish, D. D.; Roberts, J. M.; Sueper, D. T.; Atlas, E. L.; Donnelly, S. G.; Flocke, F.; Fried, A.; Potter, W. T.; Schaubler, S.; Stroud, V.; Weinheimer, A. J.; Wert, B. P.; Wiedinmyer, C.; Alvarez, R. J.; Banta, R. M.; Darby, L. S.; Senff, C. J. Effect of petrochemical industrial emissions of reactive alkenes and NO_x on tropospheric ozone formation in Houston, Texas. *Journal of Geophysical Research: Atmospheres* **2003**, *108* (D8), 4249.

(47) Wert, B. P.; Trainer, M.; Fried, A.; Ryerson, T. B.; Henry, B.; Potter, W.; Angevine, W. M.; Atlas, E.; Donnelly, S. G.; Fehsenfeld, F. C.; Frost, G. J.; Goldan, P. D.; Hansel, A.; Holloway, J. S.; Hubler, G.; Kuster, W. C.; Nicks, D. K., Jr.; Neuman, J. A.; Parrish, D. D.; Schaubler, S.; Stutz, J.; Sueper, D. T.; Wiedinmyer, C.; Wisthaler, A. Signatures of terminal alkene oxidation in airborne formaldehyde measurements during TexAQS 2000. *Journal of Geophysical Research: Atmospheres* **2003**, *108* (D3), 4104.

(48) Darby, L. S. Cluster Analysis of Surface Winds in Houston, Texas, and the Impact of Wind Patterns on Ozone. *Journal of Applied Meteorology* **2005**, *44* (12), 1788–1806.

(49) Kleinman, L. I.; Daum, P. H.; Imre, D.; Lee, Y.-N.; Nunnermacker, L. J.; Springston, S. R.; Weinstein-Lloyd, J.; Rudolph, J. Ozone production rate and hydrocarbon reactivity in 5 urban areas: A cause of high ozone concentration in Houston. *Geophysical Research Letters* **2002**, *29* (10), 105-1–105-4.

(50) Parrish, D. D.; Ryerson, T. B.; Mellqvist, J.; Johansson, J.; Fried, A.; Richter, D.; Walega, J. G.; Washenfelder, R. A.; de Gouw, J. A.; Peischl, J.; Aikin, K. C.; McKeen, S. A.; Frost, G. J.; Fehsenfeld, F. C.; Herndon, S. C. Primary and secondary sources of formaldehyde in urban atmospheres: Houston Texas region. *Atmospheric Chemistry and Physics* **2012**, *12* (7), 3273–3288.

(51) Parrish, D. D.; Allen, D. T.; Bates, T. S.; Estes, M.; Fehsenfeld, F. C.; Feingold, G.; Ferrare, R.; Hardesty, R. M.; Meagher, J. F.; Nielsen-Gammon, J. W.; Pierce, R. B.; Ryerson, T. B.; Seinfeld, J. H.; Williams, E. J. Overview of the Second Texas Air Quality Study (TexAQS II) and the Gulf of Mexico Atmospheric Composition and Climate Study (GoMACCS). *Journal of Geophysical Research: Atmospheres* **2009**, *114*, No. D00F13.

(52) Zhou, W.; Cohan, D. S.; Henderson, B. H. Slower ozone production in Houston, Texas following emission reductions: evidence from Texas Air Quality Studies in 2000 and 2006. *Atmospheric Chemistry and Physics* **2014**, *14* (6), 2777–2788.

(53) Sourì, A. H.; Choi, Y.; Li, X.; Kotsakis, A.; Jiang, X. A 15-year climatology of wind pattern impacts on surface ozone in Houston, Texas. *Atmospheric Research* **2016**, *174-175*, 124–134.

(54) Lefer, B.; Rappenglück, B.; Flynn, J.; Haman, C. Photochemical and meteorological relationships during the Texas-II Radical and Aerosol Measurement Project (TRAMP). *Atmospheric Environment* **2010**, *44* (33), 4005–4013.

(55) Liu, J.; Clark, L. P.; Bechle, M. J.; Hajat, A.; Kim, S. Y.; Robinson, A. L.; Sheppard, L.; Szpiro, A. A.; Marshall, J. D. Disparities in Air Pollution Exposure in the United States by Race/Ethnicity and Income, 1990–2010. *Environmental Health Perspectives* **2021**, *129* (12), No. 127005.

(56) Mazzuca, G. M.; Ren, X.; Loughner, C. P.; Estes, M.; Crawford, J. H.; Pickering, K. E.; Weinheimer, A. J.; Dickerson, R. R. Ozone production and its sensitivity to NO_x and VOCs: results from the DISCOVER-AQ field experiment, Houston 2013. *Atmospheric Chemistry and Physics* **2016**, *16* (22), 14463–14474.

(57) Crooks, J. L.; Licker, R.; Hollis, A. L.; Ekwurzel, B. The ozone climate penalty, NAAQS attainment, and health equity along the Colorado Front Range. *Journal of Exposure Science & Environmental Epidemiology* **2022**, *32* (4), 545–553.

- (58) Wang, Y.; Bastien, L.; Jin, L.; Harley, R. A. Location-Specific Control of Precursor Emissions to Mitigate Photochemical Air Pollution. *Environmental Science & Technology* **2023**, *57* (26), 9693–9701.
- (59) van Geffen, J. H. G.; Boersma, K. F.; Eskes, H. J.; Maasackers, J. D.; Veeffkind, J. P. TROPOMI ATBD of the total and tropospheric NO₂ data products; <http://www.tropomi.eu> (2024-05-12).
- (60) Veeffkind, J. P.; Aben, I.; McMullan, K.; Förster, H.; de Vries, J.; Otter, G.; Claas, J.; Eskes, H. J.; de Haan, J. F.; Kleipool, Q.; van Weele, M.; Hasekamp, O.; Hoogeveen, R.; Landgraf, J.; Snel, R.; Tol, P.; Ingmann, P.; Voors, R.; Kruizinga, B.; Vink, R.; Visser, H.; Levelt, P. F. TROPOMI on the ESA Sentinel-5 Precursor: A GMES mission for global observations of the atmospheric composition for climate, air quality and ozone layer applications. *Remote Sensing of Environment* **2012**, *120*, 70–83.
- (61) Boersma, K. F.; Eskes, H. J.; Dirksen, R. J.; van der A, R. J.; Veeffkind, J. P.; Stammes, P.; Huijnen, V.; Kleipool, Q. L.; Sneep, M.; Claas, J.; Leitão, J.; Richter, A.; Zhou, Y.; Brunner, D. An improved tropospheric NO₂ column retrieval algorithm for the Ozone Monitoring Instrument. *Atmospheric Measurement Techniques* **2011**, *4* (9), 1905–1928.
- (62) Boersma, K. F.; Eskes, H. J.; Richter, A.; De Smedt, I.; Lorente, A.; Beirle, S.; van Geffen, J. H. G. M.; Zara, M.; Peters, E.; Van Roozendaal, M.; Wagner, T.; Maasackers, J. D.; van der A, R. J.; Nightingale, J.; De Rudder, A.; Irie, H.; Pinardi, G.; Lambert, J. C.; Compernelle, S. C. Improving algorithms and uncertainty estimates for satellite NO₂ retrievals: results from the quality assurance for the essential climate variables (QA4ECV) project. *Atmospheric Measurement Techniques* **2018**, *11* (12), 6651–6678.
- (63) Lorente, A.; Folkert Boersma, K.; Yu, H.; Dörner, S.; Hilboll, A.; Richter, A.; Liu, M.; Lamsal, L. N.; Barkley, M.; De Smedt, I.; Van Roozendaal, M.; Wang, Y.; Wagner, T.; Beirle, S.; Lin, J. T.; Krotkov, N.; Stammes, P.; Wang, P.; Eskes, H. J.; Krol, M. Structural uncertainty in air mass factor calculation for NO₂ and HCHO satellite retrievals. *Atmospheric Measurement Techniques* **2017**, *10* (3), 759–782.
- (64) van Geffen, J. H. G. M.; Boersma, K. F.; Van Roozendaal, M.; Hendrick, F.; Mahieu, E.; De Smedt, I.; Sneep, M.; Veeffkind, J. P. Improved spectral fitting of nitrogen dioxide from OMI in the 405–465 nm window. *Atmospheric Measurement Techniques* **2015**, *8* (4), 1685–1699.
- (65) Zara, M.; Boersma, K. F.; De Smedt, I.; Richter, A.; Peters, E.; van Geffen, J. H. G. M.; Beirle, S.; Wagner, T.; Van Roozendaal, M.; Marchenko, S.; Lamsal, L. N.; Eskes, H. J. Improved slant column density retrieval of nitrogen dioxide and formaldehyde for OMI and GOME-2A from QA4ECV: intercomparison, uncertainty characterisation, and trends. *Atmospheric Measurement Techniques* **2018**, *11* (7), 4033–4058.
- (66) Boersma, K. F.; Eskes, H. J.; Brinksma, E. J. Error analysis for tropospheric NO₂ retrieval from space. *Journal of Geophysical Research: Atmospheres* **2004**, *109*, No. D04311.
- (67) Lama, S.; Houweling, S.; Boersma, K. F.; Eskes, H.; Aben, I.; Denier van der Gon, H. A. C.; Krol, M. C.; Dolman, H.; Borsdorff, T.; Lorente, A. Quantifying burning efficiency in megacities using the NO₂/CO ratio from the Tropospheric Monitoring Instrument (TROPOMI). *Atmospheric Chemistry and Physics* **2020**, *20* (17), 10295–10310.
- (68) Eskes, H. J.; Boersma, K. F. Averaging kernels for DOAS total-column satellite retrievals. *Atmospheric Chemistry and Physics* **2003**, *3* (5), 1285–1291.
- (69) Bechle, M. J.; Millet, D. B.; Marshall, J. D. Remote sensing of exposure to NO₂: Satellite versus ground-based measurement in a large urban area. *Atmospheric Environment* **2013**, *69*, 345–353.
- (70) Ludewig, A.; Kleipool, Q.; Bartstra, R.; Landzaat, R.; Leloux, J.; Loots, E.; Meijering, P.; van der Plas, E.; Rozemeijer, N.; Vonk, F.; Veeffkind, P. In-flight calibration results of the TROPOMI payload on board the Sentinel-5 Precursor satellite. *Atmospheric Measurement Techniques* **2020**, *13* (7), 3561–3580.
- (71) Eskes, H. J.; Eichmann, K.-U. *SSP Mission Performance Centre Nitrogen Dioxide [L2_NO2_] Readme*, SSP-MPC-KNMI-PRF-NO2; Copernicus, 2023.
- (72) Kowalewski, M. G.; Janz, S. J. Remote sensing capabilities of the GEO-CAPE airborne simulator. In *SPIE Optical Engineering + Applications*; SPIE, 2014; p 12.
- (73) Judd, L. M.; Al-Saadi, J. A.; Janz, S. J.; Kowalewski, M. G.; Pierce, R. B.; Szykman, J. J.; Valin, L. C.; Swap, R.; Cede, A.; Mueller, M.; Tiefengraber, M.; Abuhassan, N.; Williams, D. Evaluating the impact of spatial resolution on tropospheric NO₂ column comparisons within urban areas using high-resolution airborne data. *Atmospheric Measurement Techniques* **2019**, *12* (11), 6091–6111.
- (74) Nowlan, C. R.; Liu, X.; Janz, S. J.; Kowalewski, M. G.; Chance, K.; Follette-Cook, M. B.; Fried, A.; González Abad, G.; Herman, J. R.; Judd, L. M.; Kwon, H. A.; Loughner, C. P.; Pickering, K. E.; Richter, D.; Spinei, E.; Walega, J.; Weibring, P.; Weinheimer, A. J. Nitrogen dioxide and formaldehyde measurements from the GEostationary Coastal and Air Pollution Events (GEO-CAPE) Airborne Simulator over Houston, Texas. *Atmospheric Measurement Techniques* **2018**, *11* (11), 5941–5964.
- (75) Nowlan, C. R.; Liu, X.; Leitch, J. W.; Chance, K.; González Abad, G.; Liu, C.; Zoogman, P.; Cole, J.; Delker, T.; Good, W.; Murcray, F.; Ruppert, L.; Soo, D.; Follette-Cook, M. B.; Janz, S. J.; Kowalewski, M. G.; Loughner, C. P.; Pickering, K. E.; Herman, J. R.; Beaver, M. R.; Long, R. W.; Szykman, J. J.; Judd, L. M.; Kelley, P.; Luke, W. T.; Ren, X.; Al-Saadi, J. A. Nitrogen dioxide observations from the Geostationary Trace gas and Aerosol Sensor Optimization (GeoTASO) airborne instrument: Retrieval algorithm and measurements during DISCOVER-AQ Texas 2013. *Atmospheric Measurement Techniques* **2016**, *9* (6), 2647–2668.
- (76) Royal Belgian Institute for Space Aeronomy. QDOAS; <https://uv-vis.aeronomie.be/software/QDOAS/> (accessed 2023-11-18).
- (77) Judd, L. M.; Al-Saadi, J. A.; Szykman, J. J.; Valin, L. C.; Janz, S. J.; Kowalewski, M. G.; Eskes, H. J.; Veeffkind, J. P.; Cede, A.; Mueller, M.; Gebetsberger, M.; Swap, R.; Pierce, R. B.; Nowlan, C. R.; Abad, G. G.; Nehrir, A.; Williams, D. Evaluating Sentinel-5P TROPOMI tropospheric NO₂ column densities with airborne and Pandora spectrometers near New York City and Long Island Sound. *Atmospheric Measurement Techniques* **2020**, *13*, 6113–6140.
- (78) Keller, C. A.; Knowland, K. E.; Duncan, B. N.; Liu, J.; Anderson, D. C.; Das, S.; Lucchesi, R. A.; Lundgren, E. W.; Nicely, J. M.; Nielsen, E.; Ott, L. E.; Saunders, E.; Strode, S. A.; Wales, P. A.; Jacob, D. J.; Pawson, S. Description of the NASA GEOS Composition Forecast Modeling System GEOS-CF v1.0. *Journal of Advances in Modeling Earth Systems* **2021**, *13* (4), No. e2020MS002413.
- (79) Herman, J.; Cede, A.; Spinei, E.; Mount, G.; Tzortziou, M.; Abuhassan, N. NO₂ column amounts from ground-based Pandora and MFDOAS spectrometers using the direct-sun DOAS technique: Intercomparisons and application to OMI validation. *Journal of Geophysical Research: Atmospheres* **2009**, *114*, No. D13307.
- (80) U. S. Environmental Protection Agency. *Air Quality System*; [aqsweb/documents/data_api.html](https://www.epa.gov/aqsweb/documents/data_api.html) (accessed 2023-11-18).
- (81) Winer, A. M.; Peters, J. W.; Smith, J. P.; Pitts, J. N. Response of commercial chemiluminescent nitric oxide-nitrogen dioxide analyzers to other nitrogen-containing compounds. *Environmental Science & Technology* **1974**, *8* (13), 1118–1121.
- (82) Dunlea, E. J.; Herndon, S. C.; Nelson, D. D.; Volkamer, R. M.; San Martini, F.; Sheehy, P. M.; Zahniser, M. S.; Shorter, J. H.; Wormhoudt, J. C.; Lamb, B. K.; Allwine, E. J.; Gaffney, J. S.; Marley, N. A.; Grutter, M.; Marquez, C.; Blanco, S.; Cardenas, B.; Retama, A.; Ramos Villegas, C. R.; Kolb, C. E.; Molina, L. T.; Molina, M. J. Evaluation of nitrogen dioxide chemiluminescence monitors in a polluted urban environment. *Atmospheric Chemistry and Physics* **2007**, *7* (10), 2691–2704.
- (83) Williams, E. J.; Baumann, K.; Roberts, J. M.; Bertman, S. B.; Norton, R. B.; Fehsenfeld, F. C.; Springston, S. R.; Nunnermacker, L. J.; Newman, L.; Olszyna, K.; Meagher, J.; Hartsell, B.; Edgerton, E.; Pearson, J. R.; Rodgers, M. O. Intercomparison of ground-based NO₂

measurement techniques. *Journal of Geophysical Research: Atmospheres* **1998**, *103* (D17), 22261–22280.

(84) Russell, A. R.; Valin, L. C.; Bucsele, E. J.; Wenig, M. O.; Cohen, R. C. Space-based Constraints on Spatial and Temporal Patterns of NO_x Emissions in California, 2005–2008. *Environmental Science & Technology* **2010**, *44* (9), 3608–3615.

(85) Texas Commission on Environmental Quality. *Air Quality Forecast and Ozone Action Day Alerts*; https://www.tceq.texas.gov/airquality/monops/ozone_email.html (accessed 2023-11-18).

(86) Spielman, S. E.; Folch, D.; Nagle, N. Patterns and causes of uncertainty in the American Community Survey. *Applied Geography* **2014**, *46*, 147–157.

(87) U. S. Census Bureau. *Understanding and Using American Community Survey Data: What All Data Users Need to Know*; U. S. Department of Commerce, U. S. Census Bureau: Washington, DC, 2020.

(88) Clark, L. P.; Millet, D. B.; Marshall, J. D. Changes in Transportation-Related Air Pollution Exposures by Race-Ethnicity and Socioeconomic Status: Outdoor Nitrogen Dioxide in the United States in 2000 and 2010. *Environmental Health Perspectives* **2017**, *125* (9), No. 097012.

(89) Sun, K.; Zhu, L.; Cady-Pereira, K.; Chan Miller, C.; Chance, K.; Clarisse, L.; Coheur, P. F.; González Abad, G.; Huang, G.; Liu, X.; Van Damme, M.; Yang, K.; Zondlo, M. A physics-based approach to oversample multi-satellite, multispecies observations to a common grid. *Atmospheric Measurement Techniques* **2018**, *11* (12), 6679–6701.

(90) Clarisse, L.; Van Damme, M.; Clerbaux, C.; Coheur, P. F. Tracking down global NH₃ point sources with wind-adjusted superresolution. *Atmospheric Measurement Techniques* **2019**, *12* (10), 5457–5473.

(91) Valin, L. C.; Russell, A. R.; Cohen, R. C. Variations of OH radical in an urban plume inferred from NO₂ column measurements. *Geophysical Research Letters* **2013**, *40* (9), 1856–1860.

(92) de Foy, B.; Lu, Z.; Streets, D. G.; Lamsal, L. N.; Duncan, B. N. Estimates of power plant NO_x emissions and lifetimes from OMI NO₂ satellite retrievals. *Atmospheric Environment* **2015**, *116*, 1–11.

(93) Lu, Z.; Streets, D. G.; de Foy, B.; Lamsal, L. N.; Duncan, B. N.; Xing, J. Emissions of nitrogen oxides from US urban areas: estimation from Ozone Monitoring Instrument retrievals for 2005–2014. *Atmospheric Chemistry and Physics* **2015**, *15* (18), 10367–10383.

(94) Clark, L. P.; Harris, M. H.; Apte, J. S.; Marshall, J. D. National and Intraurban Air Pollution Exposure Disparity Estimates in the United States: Impact of Data-Aggregation Spatial Scale. *Environmental Science & Technology* **2022**, *9* (9), 786–791.

(95) De Smedt, L.; Pinardi, G.; Vigouroux, C.; Compernelle, S.; Bais, A.; Benavent, N.; Boersma, F.; Chan, K. L.; Donner, S.; Eichmann, K. U.; Hedelt, P.; Hendrick, F.; Irie, H.; Kumar, V.; Lambert, J. C.; Langerock, B.; Lerot, C.; Liu, C.; Loyola, D.; PETERS, A.; Richter, A.; Rivera Cárdenas, C.; Romahn, F.; Ryan, R. G.; Sinha, V.; Theys, N.; Vlietinck, J.; Wagner, T.; Wang, T.; Yu, H.; Van Roozendael, M. Comparative assessment of TROPOMI and OMI formaldehyde observations and validation against MAX-DOAS network column measurements. *Atmospheric Chemistry and Physics* **2021**, *21* (16), 12561–12593.

(96) Li, J.; Wang, Y.; Zhang, R.; Smeltzer, C.; Weinheimer, A.; Herman, J.; Boersma, K. F.; Celarier, E. A.; Long, R. W.; Szykman, J. J.; Delgado, R.; Thompson, A. M.; Knepp, T. N.; Lamsal, L. N.; Janz, S. J.; Kowalewski, M. G.; Liu, X.; Nowlan, C. R. Comprehensive evaluations of diurnal NO₂ measurements during DISCOVER-AQ 2011: effects of resolution-dependent representation of NO_x emissions. *Atmospheric Chemistry and Physics* **2021**, *21* (14), 11133–11160.

(97) Zoogman, P.; Liu, X.; Suleiman, R. M.; Pennington, W. F.; Flittner, D. E.; Al-Saadi, J. A.; Hilton, B. B.; Nicks, D. K.; Newchurch, M. J.; Carr, J. L.; Janz, S. J.; Andraschko, M. R.; Arola, A.; Baker, B. D.; Canova, B. P.; Chan Miller, C.; Cohen, R. C.; Davis, J. E.; Dussault, M. E.; Edwards, D. P.; Fishman, J.; Ghulam, A.; González Abad, G.; Grutter, M.; Herman, J. R.; Houck, J.; Jacob, D. J.; Joiner, J.; Kerridge, B. J.; Kim, J.; Krotkov, N. A.; Lamsal, L.; Li, C.; Lindfors, A.;

Martin, R. V.; McElroy, C. T.; McLinden, C.; Natraj, V.; Neil, D. O.; Nowlan, C. R.; O'Sullivan, E. J.; Palmer, P. I.; Pierce, R. B.; Pippin, M. R.; Saiz-Lopez, A.; Spurr, R. J. D.; Szykman, J. J.; Torres, O.; Veeckind, J. P.; Veihelmann, B.; Wang, H.; Wang, J.; Chance, K. Tropospheric emissions: Monitoring of pollution (TEMPO). *Journal of Quantitative Spectroscopy and Radiative Transfer* **2017**, *186*, 17–39.

(98) Wang, Y.; Apte, J. S.; Hill, J. D.; Ivey, C. E.; Patterson, R. F.; Robinson, A. L.; Tessum, C. W.; Marshall, J. D. Location-specific strategies for eliminating US national racial-ethnic PM_{2.5} exposure inequality. *Proceedings of the National Academy of Sciences U. S. A.* **2022**, *119* (44), No. e2205548119.

(99) Banta, R. M.; Senff, C. J.; Nielsen-Gammon, J.; Darby, L. S.; Ryerson, T. B.; Alvarez, R. J.; Sandberg, S. P.; Williams, E. J.; Trainer, M. A Bad Air Day in Houston. *Bulletin of the American Meteorological Society* **2005**, *86* (5), 657–670.

(100) Ngan, F.; Byun, D. Classification of Weather Patterns and Associated Trajectories of High-Ozone Episodes in the Houston–Galveston–Brazoria Area during the 2005/06 TexAQS-II. *Journal of Applied Meteorology and Climatology* **2011**, *50* (3), 485–499.

(101) Bernier, C.; Wang, Y.; Estes, M.; Lei, R.; Jia, B.; Wang, S.-C.; Sun, J. Clustering Surface Ozone Diurnal Cycles to Understand the Impact of Circulation Patterns in Houston, TX. *Journal of Geophysical Research: Atmospheres* **2019**, *124* (23), 13457–13474.

(102) Davis, J. M.; Eder, B. K.; Nychka, D.; Yang, Q. Modeling the effects of meteorology on ozone in Houston using cluster analysis and generalized additive models. *Atmospheric Environment* **1998**, *32* (14), 2505–2520.

(103) Rappenglück, B.; Perna, R.; Zhong, S.; Morris, G. A. An analysis of the vertical structure of the atmosphere and the upper-level meteorology and their impact on surface ozone levels in Houston, Texas. *Journal of Geophysical Research: Atmospheres* **2008**, *113*, No. D17315.

(104) *CalinskiHarabaszEvaluation*; <https://www.mathworks.com/help/stats/clustering.evaluation.calinskiharabaszevaluation.html#bt07j9e> (accessed 2024-06-26).

(105) De Landtsheer, S. *kmeans_opt*; https://www.mathworks.com/matlabcentral/fileexchange/65823-kmeans_opt (accessed 2024-06-26).

(106) Hastie, T.; Tibshirani, R.; Friedman, J. *The Elements of Statistical Learning*; Springer New York Inc.: New York, NY, 2001.

(107) Zuur, A. F.; Ieno, E. N.; Walker, N.; Saveliev, A. A.; Smith, G. M. *Mixed Effects Models and Extensions in Ecology with R*; Springer: New York, NY, 2009.

(108) Barmpadimos, I.; Keller, J.; Oderbolz, D.; Hueglin, C.; Prévôt, A. S. H. One decade of parallel fine (PM_{2.5}) and coarse (PM_{10-PM_{2.5}}) particulate matter measurements in Europe: Trends and variability. *Atmospheric Chemistry and Physics* **2012**, *12* (7), 3189–3203.

(109) Zheng, J.; Swall, J. L.; Cox, W. M.; Davis, J. M. Interannual variation in meteorologically adjusted ozone levels in the eastern United States: A comparison of two approaches. *Atmospheric Environment* **2007**, *41* (4), 705–716.

(110) Gao, Z.; Ivey, C. E.; Blanchard, C. L.; Do, K.; Lee, S.-M.; Russell, A. G. Separating emissions and meteorological impacts on peak ozone concentrations in Southern California using generalized additive modeling. *Environmental Pollution* **2022**, *307*, No. 119503.

(111) Pusede, S. E.; Steiner, A. L.; Cohen, R. C. Temperature and Recent Trends in the Chemistry of Continental Surface Ozone. *Chemical Reviews* **2015**, *115* (10), 3898–3918.

(112) Pusede, S. E.; Cohen, R. C. On the observed response of ozone to NO_x and VOC reactivity reductions in San Joaquin Valley California 1995–present. *Atmospheric Chemistry and Physics* **2012**, *12* (18), 8323–8339.

(113) Daum, P. H.; Kleinman, L. I.; Springston, S. R.; Nunnermacker, L. J.; Lee, Y.-N.; Weinstein-Lloyd, J.; Zheng, J.; Berkowitz, C. M. A comparative study of O₃ formation in the Houston urban and industrial plumes during the 2000 Texas Air Quality Study. *Journal of Geophysical Research: Atmospheres* **2003**, *108* (D23), 4715.

(114) Neuman, J. A.; Nowak, J. B.; Zheng, W.; Flocke, F.; Ryerson, T. B.; Trainer, M.; Holloway, J. S.; Parrish, D. D.; Frost, G. J.; Peischl, J.; Atlas, E. L.; Bahreini, R.; Wollny, A. G.; Fehsenfeld, F. C. Relationship between photochemical ozone production and NO_x oxidation in Houston, Texas. *Journal of Geophysical Research: Atmospheres* **2009**, *114*, No. D00F08.

(115) Tessum, C. W.; Paoletta, D. A.; Chambliss, S. E.; Apte, J. S.; Hill, J. D.; Marshall, J. D. PM_{2.5} pollutants disproportionately and systemically affect people of color in the United States. *Science Advances* **2021**, *7* (18), No. eabf4491.

(116) Thind, M. P. S.; Tessum, C. W.; Azevedo, I. L.; Marshall, J. D. Fine Particulate Air Pollution from Electricity Generation in the US: Health Impacts by Race, Income, and Geography. *Environmental Science & Technology* **2019**, *53* (23), 14010–14019.

(117) Pluecker, J. Flashpoints on the Road to Black and Brown Power: Site of Struggle in Houston in 1960s and 70s. *Rice Design Alliance Summer*; Rice University, 2010; pp 30–31; https://offcite.rice.edu/2010/07/Cite_83_Flashpoints-on-the-Road-to-Black-and-Brown-Power.pdf.

(118) Turner, M. A.; Santos, R.; Levy, D. K.; Wissoker, D.; Aranda, C.; Pittingolo, R. *Housing Discrimination against Racial and Ethnic Minorities 2012: Full Report*; U.S. Department of Housing and Urban Development, Office of Policy Development and Research, 2013.

(119) U.S. Department of Housing and Urban Development, Fort Worth Regional Office, Region VI Office of Fair Housing & Equal Opportunity. *Letter Finding Noncompliance with Title VI of the Civil Rights Act of 1964*; Case Number: 06-16-R001-6; January 11, 2017.

(120) *Segregation by Design: An atlas of redlining, "urban renewal," and environmental racism*; <https://www.segregationbydesign.com/houston/redlining> (accessed 2024-04-18).

(121) Zuvanich, A. TxDOT holding public meetings in Houston ahead of construction for I-45 expansion project. *Houston Public Media* December 6, 2023; <https://www.houstonpublicmedia.org/articles/news/transportation/2023/12/06/471658/txdot-holding-public-meetings-in-houston-ahead-of-construction-for-i-45-expansion-project/>.

(122) *Revisions to the State of Texas Air Quality Implementation Plan for the Control of Ozone Air Pollution: Dallas-Fort Worth and Houston-Galveston-Brazoria 2015 Eight Hour Ozone Standard Nonattainment Areas Proposal*; 2022-023-SIP-NR; Texas Commission on Environmental Quality, 2023.

(123) London, J. K.; Nguyen, P.; Dawson, M.; Manrique, K. *Community Engagement in AB 617: An Evaluation of Challenges, Successes, Lessons Learned and Recommendations for the Future*; UC Davis, 2020.

(124) Air Alliance Houston. *Local Policy Recommendations Addressing Environmental Hazards and Inequitable Health Risks in Houston's Complete Communities*; 2019.

(125) *Southern Crushed Concrete, LLC v. City of Houston*; Texas, Supreme Court of Texas, June 13, 2013; Vol. 56 Tex. Sup. Ct. J. 295 (Tex. 2013), 56 Tex. Sup. Ct. J. 295.

(126) *BCCA Appeal Grp., Inc. v. City of Houston*; Supreme Court of Texas, S. C. April 29, 2016; Vol. 496 S.W.3d 1 (Tex. 2016).

(127) Texas Commission on Environmental Quality. *Texas State Implementation Plan*; <https://www.tceq.texas.gov/airquality/sip> (accessed 2024-06-26).

(128) Manson, S.; Schroeder, J.; Van Riper, D.; Knowles, K.; Kugler, T.; Roberts, F.; Ruggles, S. *IPUMS National Historical Geographic Information System: Version 18.0 [dataset]*; IPUMS: Minneapolis, MN, 2023.